Optimization for Active Learning-based Interactive Database Exploration

Enhui Huang, Liping Peng, Luciano Di Palma, Ahmed Abdelkafi, Anna Liu, Yanlei Diao

Optimization for Active Learning-based Interactive Database Exploration

Enhui Huang[†], Liping Peng[*], Luciano Di Palma[†], Ahmed Abdelkafi[†], Anna Liu[*], Yanlei Diao[*,†]
[†] Ecole Polytechnique, France; [*]University of Massachusetts Amherst, USA

[†]{enhui.huang, luciano.di-palma, ahmed.abdelkafi}@polytechnique.edu,
[*]{lppeng, yanlei}@cs.umass.edu, anna@math.umass.edu

ABSTRACT

There is an increasing gap between the fast growth of data and the limited human ability to comprehend data. Consequently, there has been a growing demand of data management tools that can bridge this gap and help the user retrieve high-value content from data more effectively. In this work, we aim to build interactive data exploration as a new database service, using an approach called "explore-by-example". In particular, we cast the explore-by-example problem in a principled "active learning" framework, and bring the properties of important classes of database queries to bear on the design of new algorithms and optimizations for active learning-based database exploration. These new techniques allow the database system to overcome fundamental limitations of traditional active learning, in particular, the slow convergence problem. Evaluation results using real-world datasets and user interest patterns show that our new system significantly outperforms state-of-the-art active learning techniques and data exploration systems in accuracy while achieving desired efficiency for interactive performance.

1. INTRODUCTION

Today data is being generated at an unprecedented rate. However, the human ability to comprehend data remains as limited as before. Consequently, there has been a growing demand of data management tools that can bridge the gap between the data growth and limited human ability, and help retrieve high-value content from data more effectively.

To respond to such needs, we build a new database service for interactive exploration in a framework called "*explore-by-example*" [13, 14]. In this framework, the database content is considered as a set of tuples, and the user is interested in some of them but not all. In the data exploration process, the system allows the user to interactively label tuples as "interesting" or "not interesting", so that it can construct an increasingly-more-accurate model of the user interest. Eventually, the model is turned into a *user interest query*[1] that will retrieve all relevant tuples from the database.

In this work, we consider the following examples as our target applications. First, when a scientist comes to explore a large sky survey database such as SDSS [41], she may not be able to express her data interest precisely. Instead, she may prefer to navigate through a region of the sky, see a few examples of sky objects, provide yes or no feedback, and ask the system to find all other (potentially many more) relevant sky objects from the database. Second, consider many web applications backed by a large database, such as E-commerce websites and housing websites, which provide a simple search interface for everyday users but leave the job of filtering through a long list of returned objects to the user. The new database service in the explore-by-example framework will provide these applications with a new way to interact with the user and, more importantly, help the user filter through numerous objects more efficiently. Additional applications have been discussed in prior work on explore-by-example [13, 14].

Our approach to building an explore-by-example system is to cast it in an "*active learning*" framework: We treat the modeling of the user interest as a *classification* problem where all the user labeled examples thus far are used to train a classification model. Then active learning [5, 37, 43] decides how to choose a new example, from the unlabeled database, for the user to label next so that the system can learn the user interest efficiently.

The active learning based explore-by-example approach offers potential benefits over alternative methods such as faceted search [27, 35, 36] and semantic windows [26] for several reasons.

First, the user interest may include varying degrees of complexity, or the user does not have prior knowledge about the complexity and hence requires the system to have the flexibility to learn a model as complex as necessary for his interest. More specifically, if the user knows the relevant attributes and just wants to set the appropriate value for each attribute, an interactive GUI or faceted search [27, 35, 36] may be sufficient. However, the user interest may involve more complex constraints, e.g., "$(\frac{rowc-a_1}{b_1})^2 + (\frac{rowc-a_2}{b_2})^2 < c$", and "$x + 2.5 * \log_{10}(y) < 23.3$" from the SDSS example query set [40], or "$length * width > c$" as seen in our car database. If the user knows the function shape and constants in advance, some of the above examples (e.g., the ellipse pattern) can be supported by semantic windows [26] as pre-defined patterns. However, if the user does not have such prior knowledge, explore-by-example may work regardless of how complex the predicates are, and which functions and constants are used in the predicates.

Second, increased dimensionality makes it harder for semantic windows to scale. For example, when the interest of the SDSS user involves both the ellipse and log patterns above, it will be more difficult for both the system and the user to handle multiple patterns for data exploration (even if such patterns can be predefined). In contrast, as the dimensionality increases, explore-by-example can keep the same user interface for data exploration and handles increased complexity via its learning algorithm "behind the scenes".

While prior work on explore-by-example has used active learning [14], a main issue is the large number of labeled examples needed to achieve high accuracy. For example, 300-500 labeled examples are needed to reach 80% accuracy [14], which is undesirable in many applications. This problem, referred to as *slow convergence*, is exacerbated when the user interest covers only a small fraction of the database (i.e., low selectivity) or the number of the

[1] In our work we use the term, *user interest query*, to refer to the final query that represents the user interest, while the term, *user interest model*, can refer to an immediate model before it converges to the true user interest.

attributes chosen for exploration is large (i.e., high dimensionality).

In this work, we take a new approach to active learning-based database exploration. Instead of improving active learning in isolation from the database, we treat it as an internal module of the database system and ask the question: *what query and data properties from the database can we leverage to address the slow convergence problem?* Based on the common properties that we observed in query traces from the Sloan Digital Sky Survey [40] and a car database (described more in Section 6), we can indeed design new techniques that overcome or alleviate the slow convergence problem. Some of the key query properties include:

Subspatial Convexity: Consider the database attributes as dimensions of a data space $\mathcal{D}$ and map the tuples to the space based on the values of their attributes. Then all the tuples that match the user interest form the positive region in $\mathcal{D}$; others form the negative region. We observe that in some lower-dimensional subspaces of $\mathcal{D}$, the projected positive or negative region is a convex object. For example, the SDSS query trace [40] includes 116 predicates, among which 107 predicates define a convex positive region in the subspace formed by the attributes used in the predicate, and 3 predicates define a convex negative region in their subspaces. For the car database, the 70 predicates defined on numerical attributes all form a convex positive region. Figure 2 shows a range of predicates from these two databases and their positive and negative regions.

Conjunctivity: Conjunctive queries are a major class of database queries that have been used in numerous applications. For data exploration, we are interested in the "conjunctive" property of the set of predicates that characterize the user interest. Among 45 queries provided by SDSS [40], 40 queries are conjunctive queries. For the car database, all user queries use the conjunctive property.

In this paper, we bring the subspatial convexity and conjunctive properties of database queries, treated as true (yet unknown) user interest queries, to bear on the design of new algorithms and optimizations for active learning-based database exploration. These techniques allow the database system to overcome fundamental limitations of traditional active learning, in particular, the slow convergence problem when data exploration is performed with high dimensionality and low selectivity of the user interest query. More specifically, our paper makes the following contributions.

1. Dual-Space Model (§ 3): By leveraging the subspatial convex property, we propose a new "dual-space model" (DSM) that builds not only a classification model, $F_{\mathcal{V}}$, from labeled examples, but also a polytope model of the data space, $F_{\mathcal{D}}$. On one hand, active learning theory improves $F_{\mathcal{V}}$ by choosing the next example that enables reduction of the version space $\mathcal{V}$ (the space of all classification models consistent with labeled data). On the other hand, our polytope model offers a more direct description of the data space $\mathcal{D}$ including the areas known to be positive, areas known to be negative, and areas with unknown labels. We use both models to predict unlabeled examples and choose the best example to label next.

In addition, DSM allows us to prove exact and approximate lower bounds on the model accuracy in terms of F1-score. While recent active learning theory offers provable bounds on classification errors [7, 15, 19–21], it treats positive and negative classes equally. Given the low selectivity of user interest queries, e.g., 1%, a classifier that classifies all tuples to the negative class has a low error rate of 1%, but fails to return any relevant tuples. Therefore, we choose to bound F1-score as it emphasizes the accuracy for the positive class, i.e., the relevant tuples returned to the user.

2. High-dimensional Exploration: When the user interest involves a large number of attributes, we employ two approaches to reducing dimensionality in data exploration.

(a) *Factorization* (§ 4): By leveraging the conjunctive and subspatial convexity property of user interest queries, we factorize a high-dimensional data space into low-dimensional subspaces, in some of which the projections of user positive or negative regions are convex. Our dual-space model with factorization, DSM$_F$, runs the polytope model in each subspace where the convex property holds. We formally define the class of queries that DSM$_F$ supports, the decision function it utilizes, and prove that it achieves a better lower bound of F1-score than DSM without factorization.

(b) *Online feature selection* (§ 5): The user may start exploration with more attributes than those needed in the final model. To remove irrelevant attributes, we propose an online feature selection method that adaptively selects the top-k relevant attributes and leverages the convex property (if present) for optimization.

3. Evaluation (§ 6): We evaluated our system using two real datasets and user interest queries. The SDSS dataset [41] includes 190M tuples, for which the user interests are selective and their decision boundaries present varied complexity for detection. (1) Without knowing these queries in advance, DSM can achieve F1-score of 95% within 10 labeled examples if the decision boundary B falls in a sparse region, and otherwise requires up to 100 labeled examples for 2D queries and 160-240 examples for 4D-6D queries while maintaining per-iteration time within 1-2 seconds. (2) DSM$_F$ significantly outperforms learning methods including Active Learning (AL) [5, 16], which after 500 examples fails to reach 95% for most 2D queries and achieves only an average of 66% for 4D-6D queries, and Active Search [17], which fails to achieve F1-score more than 20% for all queries. (3) Recent explore-by-example systems, Aide [13, 14] and LifeJoin [10], fail to achieve 10% F1-score when the user interest involves 4 attributes or more.

Our user study using a 5622-tuple car database validates the subspatial convex property and the conjunctive property of user interest queries. It also shows the benefits of DSM$_F$ (a median of 10 labeled examples to reach high accuracy) over manual exploration (where the user wrote 12 queries and reviewed 98 tuples as the median), as well as over AL even in the presence of noisy user labels.

2. BACKGROUND

In this section, we review our design of an explore-by-example system and present background on active learning theory.

2.1 System Overview

Our data exploration system is depicted in Figure 1. The main concepts and modules are described as follows.

Data space. When a user comes to explore a database, she is presented with the database schema for browsing. Based on her best understanding of the (implicit) exploration goal, she may choose a set of attributes, $\{A_i\}$, $i = 1, \ldots, d$, from a table for consideration. These attributes form a superset of the relevant attributes that will eventually be discovered by the system. Let us consider the projection of the underlying table to $\{A_i\}$, and pivot the projected table such that each A_i becomes a dimension and the projected tuples are mapped to points in this d-dimensional space – the resulting space is called a *data space* where the user exploration will take place.

Initial examples. To bootstrap data exploration, the user is asked to give a positive example and a negative example. If the user does not have such examples, the system can run an initial sampling algorithm [13, 30] over the data space to help the user find such examples. Since the initial sampling problem has been studied before, our work in this paper focuses on data exploration after such initial examples are identified.

Iterative learning and exploration. The iterative exploration starts with a given positive example set and a negative example

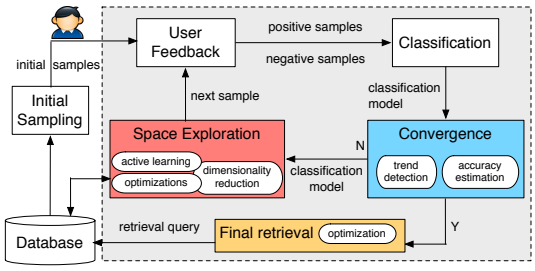

Figure 1: System architecture for explore by example.

set, which form the labeled dataset. In each iteration, the labeled dataset is used to train a user interest model, which is fast due to the small size of training data. Before the model reaches convergence or a user-specified accuracy level, it is used next to explore the data space and retrieve a new example for display. In the next iteration, the user labels this example as positive or negative – such feedback can be collected explicitly through a graphical interface [12], or implicitly based on the user behavior.[2] The newly labeled example is added to the labeled dataset, and the above process repeats.

Convergence and final retrieval. At each iteration, our system assesses the current model to decide whether more exploration iterations are needed. The process is terminated when the model accuracy has reached a user-defined threshold. At this point, the model for the positive class is translated to a query which will retrieve from the database all the tuples classified as relevant.

To provide better interpretability, our system can visualize the final (nonparametric) model and fit a corresponding parametric model, the form of which can be suggested by the user after seeing the visualization. For example, a pattern that is visually an ellipse or a hyperbola can be fitted using logistic or probit regression.

2.2 Active Learning for Data Exploration

The problem of dynamically seeking the next example for labeling from a large database of unlabeled tuples is closely related to active learning. The recent results on active learning are surveyed in [37]. Below, we summarize those results relevant to our work.

Pool-Based Sampling. Many real-world problems fit the following scenario: there is a small set of labeled data $\mathcal{L}$ and a large pool of unlabeled data $\mathcal{U}$ available. In active learning, an example is chosen from the pool in a greedy fashion, according to a utility measure used to evaluate all instances in the pool (or, if $\mathcal{U}$ is large, a subsample thereof). In our setting of database exploration, the labeled data $\mathcal{L}$ is what the user has provided thus far. The pool $\mathcal{U}$ is a subsample of size m of the unlabeled part of the database. The utility measure depends on the classifier in use, as discussed below.

Classification Model. Previous explore-by-example systems [13, 14] used decision trees to build a classification model. This approach works if the user interest pattern is a hyper-rectangle in the data space, whereas real-world applications may use more complex predicates. For the pattern in Figure 2(b), the decision tree method needs 71 range predicates to approximate the region well and uses 1800 training examples to reach 95% accuracy, which is consistent with known criticism on decision trees [22]. Hence it is undesirable due to large numbers of examples labeled by the user.

To support more complex predicates, our system employs more powerful classifiers such as Support Vector Machines (SVM) with the kernel method or Gradient Boosting. The new techniques proposed in our work do **not** depend on the specific classifier; they can work with most existing classifiers. But the implementation of active learning does depend on the classifier in use. For ease of composition, in this paper we use SVM as an example classifier.

[2]The methods for collecting user feedback are in the purview of human-computer interaction and are beyond the scope of this paper.

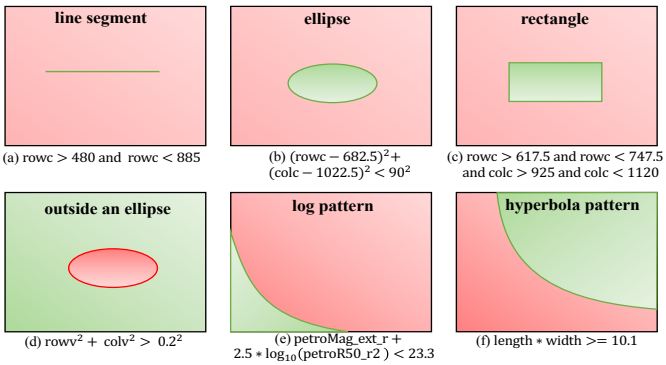

Figure 2: Positive (green) and negative (red) regions of 6 predicates

Uncertainty Sampling and Version Space Search. A common form of utility measure over the unlabeled pool $\mathcal{U}$ characterizes the degree of *uncertainty* that the current model experiences for classifying each data example in $\mathcal{U}$. Under uncertainty sampling, the example that leads to the highest degree of uncertainty in classification is chosen as the example for labeling. If the classifier is SVM-based, the uncertainty can be measured by the *distance* of each example from the decision boundary of the current SVM. To improve efficiency, recent work [5, 16] further proposed to restrict uncertainty sampling to a subsample of size $l < |\mathcal{U}|$, i.e., to choose the example closest to the current decision boundary among l examples with a probabilistic guarantee that this example is within top p% closest to the decision boundary among the pool $\mathcal{U}$. This is the sampling algorithm for SVM used in our system.

A formal description of uncertainty sampling is through the notion of *version space*, which is the space of all configurations of the classification model consistent with labeled data. Uncertainty sampling is a (rough) approximation of an optimal algorithm that bisects the version space with each selected example [43]. For the above reason, we call active learning algorithms *version space-based* because they are designed to reduce the version space.

3. DUAL-SPACE MODEL

For interactive data exploration, active learning algorithms often require a large number of user-labeled examples to reach high accuracy, known as the slow convergence problem. This is especially true when the database is large and the user interest query is selective. One reason for slow convergence is the limitation of uncertainty sampling itself: it may exert a lot of effort searching in sparse, noisy, or irrelevant regions of the input space [37].

With the goal to provide a service for database exploration, our work takes a new, a database centric approach to tackle the slow convergence problem. While active learning theory has been developed in isolation from the database in use, we consider the query traces available in a database. We observe from existing query traces that in some lower-dimensional subspaces, the projected positive or negative region of user interest query is often a convex object. In this section, we utilize such subspatial convexity and introduce a dual-space (data and version space) model, which enables improved accuracy and provable lower bounds on the model accuracy. In this section, we consider the simple case that the convex property holds for the query over the entire data space $\mathcal{D}$ without factorization and defer the extension to subspaces to §4. We call this class of queries "*convex pattern queries*", denoted as $\mathbf{Q}_c \equiv \mathbf{Q}_c^+ \cup \mathbf{Q}_c^-$. Figure 2 gives examples in both classes.

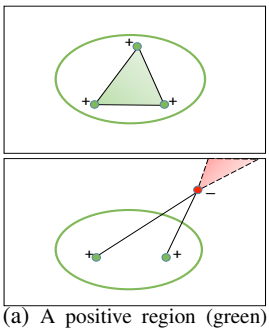

(a) A positive region (green) with 3 examples, and a negative region (red) with 1 negative and 2 positive examples

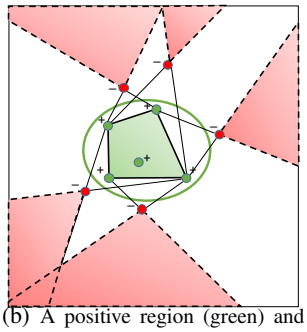

(b) A positive region (green) and 5 negative regions (red) built from 5 positive examples and 5 negative examples.

Figure 3: Examples of positive and negative regions in the polytope model.

3.1 A Polytope Model in Data Space

The key idea behind our *data space* model is that at each iteration we use all available labeled examples to build a partitioning of the data space. The partitioning divides the data space into the *positive region* (any point inside which is known to be positive), the *negative region* (any point inside which is known to be negative) and the *uncertain region*. As more labeled examples are provided, we have more knowledge about the uncertain region, so part of the uncertain region will be converted to either the positive region or the negative region in later iterations. Eventually, with enough training data, the uncertain region shrinks to the minimum, and the positive region converges to the query region.

For ease of composition, we begin with the class of queries whose positive region is convex ($\mathbf{Q}_c^+$). When the query region Q is convex, any point on the line segment connecting two points $\boldsymbol{x}_1 \in Q$ and $\boldsymbol{x}_2 \in Q$ is also in Q. Then we have the following definition.

Definition 3.1 (Positive Region) *Denote the examples that have been labeled as "positive" as $L^+ = \{e_i^+ \mid i = 1, \ldots, n^+\}$. The convex hull of L^+ is known to be the smallest convex set that contains L^+ [28] and is called the positive region, denoted as R^+.*

It is known that the convex hull of a finite number of points is a *convex polytope* [18]. For example, the green triangle in Fig. 3(a) and the green pentagon in Fig. 3(b) are the positive regions formed by three and five positive examples, respectively, which are an approximation of the query region marked by the green ellipse. We can prove the following property of the positive region for convex queries, assuming that user labels are consistent with her interest:

Proposition 3.1 *All points in the positive region R^+ are positive.*

All proofs in this paper are left to Appendix A of our technical report [23] due to space constraints.

Definition 3.2 (Negative Region) *For a negative example $\boldsymbol{e}_i^-$, we can define a corresponding negative region R_i^- such that the line segment connecting any point $\boldsymbol{x} \in R_i^-$ and $\boldsymbol{e}_i^-$ does not overlap with the positive region R^+, but the ray that starts from $\boldsymbol{x} \in R_i^-$ and passes through $\boldsymbol{e}_i^-$ will overlap with R^+. More formally, $R_i^- = \{\boldsymbol{x} | \overline{\boldsymbol{x}\boldsymbol{e}_i^-} \cap R^+ = \emptyset \wedge \overrightarrow{\boldsymbol{x}\boldsymbol{e}_i^-} \cap R^+ \neq \emptyset\}$. Given n^- negative examples, the negative region R^- is the union of the negative region for each negative example, i.e., $R^- = \cup_{i=1}^{n^-} R_i^-$.*

From the definition, we know that R_i^- is a convex cone generated by the conical combination of the vectors from the positive examples to the given negative example, i.e., $\overrightarrow{e_j^+ e_i^-}$ $(j = 1, \ldots, n^+)$. The red triangle in Fig. 3(a) depicts such a convex cone. However, the union of $R_i^-, i = 1, 2, \ldots$ is non-convex. For example, the union of the five red polygons in Fig. 3(b) is non-convex. Given more labeled examples, the result of the union will be more accurate for approximating the true negative region, which is outside the ellipse. We prove the following property of the negative region:

Proposition 3.2 *All points in the negative region R^- are negative.*

Definition 3.3 (Uncertain Region) *Denote the data space as $\mathbb{R}^d$, the uncertain region $R^u = \mathbb{R}^d - R^+ - R^-$.*

Formally, the polytope model makes a decision about an example $\boldsymbol{x}$ based on the following decision function, which takes values in $\{-1, 0, 1\}$ corresponding to R^-, R^u, and R^+ defined above:

$$F_{\mathcal{D}}(\boldsymbol{x}) = 1 \cdot \mathbb{1}(\boldsymbol{x} \in R^+) - 1 \cdot \mathbb{1}(\boldsymbol{x} \in R^-). \quad (1)$$

Our work also supports the case that the negative region of the query is convex ($\mathbf{Q}_c^-$). We can simply switch the above definitions such that we build a convex polytope for the negative region, and a union of convex cones for the positive region, one for each positive example. We also offer a test at the beginning of the data exploration process to choose between two polytope models, $Q \in \mathbf{Q}_c^+$ or $Q \in \mathbf{Q}_c^-$. The details are deferred to Section 4 where we offer a test procedure for all the assumptions made in the work.

Three-Set Metric. Our goal is not only to provide a new data space model, as described above, but also to design a new learning algorithm that enables a provable bound on the model accuracy. As stated before, our accuracy measure is F1-score. Formally, F1-score is evaluated on a *test set* $D_{test} = \{(\boldsymbol{x}_i, y_i)\}$, where $\boldsymbol{x}_i$ denotes a database object and y_i denotes its label according to the classification model. Then F1-score is defined as:

$$\text{F1-score} = 2 \cdot \frac{precision \cdot recall}{precision + recall},$$

where *precision* is the fraction of points returned by the model (query on D_{test}) that are positive, and *recall* is the fraction of positive points in D_{test} that are returned by the model.

However, capturing F1-score in our data exploration procedure is difficult because we do not have such a labeled test set, D_{test}, available. We cannot afford to ask the user to label more to produce one since the user labor is an important concern. To bound the F1-score with limited labeled data, our idea is to run our polytope model, $F_{\mathcal{D}} : \mathbb{R}^d \rightarrow \{-1, 0, 1\}$, on an evaluation set. We define the *evaluation set* D_{eval} as the projection of D_{test} without labels y_i's. Then for each data point in D_{eval}, depending on which region it falls into, D_{eval} can be partitioned into three sets accordingly, denoted as D^+, D^- and D^u. We can compute a metric from the number of data points in the three sets, as follows.

Definition 3.4 (Three-Set Metric) *Denote $D^+ = D_{eval} \cap R^+$, $D^- = D_{eval} \cap R^-$, $D^u = D_{eval} \cap R^u$, and $|S|$ means the size of set S. At a specific iteration of exploration, the three-set metric is defined to be $\frac{|D^+|}{|D^+| + |D^u|}$.*

We will prove shortly that this metric is a lower bound of F1-score evaluated on D_{test}. As more labeled examples are provided, data points will be moved from D^u to either D^+ or D^-. Eventually, with enough training data the uncertain set shrinks to an empty set and the three-set metric reaches 100%, reaching convergence.

3.2 Dual-Space Model and Algorithm

We now propose a new algorithm for interactive data exploration by exploiting models from two spaces, including our data space model $F_{\mathcal{D}}$ with the three set metric, and a classification model $F_{\mathcal{V}}$ with uncertainty sampling derived from the version space.

We first define the dual-space model (DSM) by considering two functionalities of a model used for interactive data exploration.

(1) *Prediction*: Given an unlabeled example, DSM predicts the class label first based on the data space model $F_{\mathcal{D}}$. If the example falls in the positive region R^+, it is predicted to be positive; if it falls in the negative region R^-, it is predicted to be negative. If the example falls in the unknown region R^u, then the classification model $F_{\mathcal{V}}$ is used to predict the example to be positive or negative.

(2) *Sampling*: In the active learning framework, the model is also used to guide the choice of the next example for labeling such that the new label can lead to significant improvement of the model accuracy. As discussed in Section 2, active learning uses an uncertainty sampling method, $\mathcal{S}_{\mathcal{V}}$, for a given classification model to choose the next example. However, directly application of uncertainty sampling to our dual-space model raises a problem: the example chosen by $\mathcal{S}_{\mathcal{V}}$ may fall in the known positive or negative region of our data space model $f_{\mathcal{D}}$, hence wasting computing resources on such examples. In our work, we propose an uncertainty sampling method that is restricted to the unknown region of our data space model, denoted as $\mathcal{S}_{\mathcal{D}}$. However, if we sample only from the unknown region of our data space model, we may not get a representative sample to train the classifier. Therefore, we use a sampling ratio, γ, to alternate between the sampling methods, $\mathcal{S}_{\mathcal{D}}$ and $\mathcal{S}_{\mathcal{V}}$. For instance, when $\gamma = 1/3$, in each iteration we use $\mathcal{S}_{\mathcal{D}}$ with probability 1/3 and use $\mathcal{S}_{\mathcal{V}}$ otherwise.

Now we present the full algorithm for interactive data exploration, as shown in Algorithm 1. The input is the database D, a positive example $\boldsymbol{x}^+$, a negative example $\boldsymbol{x}^-$, a user-defined accuracy threshold λ, and the sampling ratio γ. First, we extract an evaluation dataset D_{eval} from the database D (line 1). For now, let us assume D_{eval} to be D. Then we initialize data structures, setting the unknown partition of the evaluation dataset to be D_{eval}. The algorithm next goes through iterative exploration.

Lines 8-14 update our DSM model. The data space model, R^+ and R^-, is updated with the newly labeled example(s) by the user (lines 8-9). This step incrementally updates our convex polytope for R^+ and the union of convex polytopes for R^- based on computational geometry [3]. Afterwards, the corresponding partitions of D_{eval} are incrementally updated (line 10). In this step, some examples are removed from the unknown partition D^u and placed to the positive partition D^+ or the negative partition D^-. The accuracy is then estimated using the Three-Set Metric. We also keep track of the labeled and unlabeled examples using $D_{labeled}$ and $D_{unlabeled}$. We use the labeled examples to train a classifier, that is, the version space model in our DSM.

Then lines 15-28 implement uncertainty sampling using DSM. With probability γ, we perform uncertainty sampling from a pool that is restricted to the unknown partition of the evaluation set, D^u. Then the example chosen by uncertainty sampling is labeled by the user. With probability $1-\gamma$, we perform uncertainty sampling from a pool that is a subsample of all unlabeled examples in the database. Then the example chosen by uncertainty sampling is first run through our data space model, (R^+, R^-), to see if it falls in the positive or negative region and hence can be labeled directly by the model. Otherwise, it will be labeled by the user.

Then the algorithm proceeds to the next iteration. It repeats until it has met the user accuracy requirement based on the lower bound offered by our Three-Set Metric, or reached the maximum of iterations allowed (line 29). Finally, we run the DSM model over the database to retrieve all tuples predicated to be positive, for which an optimization is available but is left to [23] due to space constraints.

There are several `subsample` procedures in Algorithm 1. We discuss their optimization in Section 3.4.

Algorithm 1 Dual-Space Algorithm for Convex Queries

Input: database D, a positive example $\boldsymbol{x}^+$, a negative example $\boldsymbol{x}^-$, accuracy threshold λ, sampling ratio γ

1: $D_{eval} \leftarrow$ `subsample`(D, n)
2: $R^+ \leftarrow \emptyset$, $R^- \leftarrow \emptyset$
3: $D^+ \leftarrow \emptyset$, $D^- \leftarrow \emptyset$, $D^u \leftarrow D_{eval}$
4: $D_{labeled} \leftarrow \{\, \boldsymbol{x}^+, \boldsymbol{x}^- \}$
5: $D_{unlabeled} \leftarrow D \setminus D_{labeled}$
6: $D_{labeled\_by\_user} \leftarrow D_{labeled}$, $D_{labeled\_by\_dsm} \leftarrow \emptyset$
7: **repeat**
// building the Dual-Space model:
8: **for** $\boldsymbol{x} \in D_{labeled\_by\_user}$ **do**
9: $(R^+, R^-) \leftarrow$ `updateRegion`$(R^+, R^-, \boldsymbol{x})$
10: $(D^+, D^-, D^u) \leftarrow$ `threeSets`$(R^+, R^-, D^+, D^-, D^u)$
11: $accu \leftarrow$ `threeSetMetric`(D^+, D^-, D^u)
12: $D_{labeled}$.`append`$(D_{labeled\_by\_user} \cup D_{labeled\_by\_dsm})$
13: $D_{unlabeled}$.`remove`$(D_{labeled\_by\_user} \cup D_{labeled\_by\_dsm})$
14: $classifier \leftarrow$ `trainClassifier`$(D_{labeled})$
// uncertainty sampling:
15: $D_{labeled\_by\_user} \leftarrow \emptyset$, $D_{labeled\_by\_dsm} \leftarrow \emptyset$
16: **if** $rand() \leq \gamma$ **then**
17: $pool \leftarrow$ `subsample`(D^u, m)
18: $\boldsymbol{x} \leftarrow$ `getNextToLabel`$(pool, classifier)$
19: $D_{labeled\_by\_user} \leftarrow$ `getUserLabel`$(\boldsymbol{x})$
20: **else**
21: $pool \leftarrow$ `subsample`$(D_{unlabeled}, m)$
22: $\boldsymbol{x} \leftarrow$ `getNextToLabel`$(pool, classifier)$
23: **if** $\boldsymbol{x} \in R^+$ **then**
24: $D_{labeled\_by\_dsm} \leftarrow (\boldsymbol{x}, 1)$
25: **else if** $\boldsymbol{x} \in R^-$ **then**
26: $D_{labeled\_by\_dsm} \leftarrow (\boldsymbol{x}, -1)$
27: **else**
28: $D_{labeled\_by\_user} \leftarrow$ `getUserLabel`$(\boldsymbol{x})$
29: **until** $accu \geq \lambda$ **or** `reachedMaxNum`()
30: `finalRetrieval`$(D, (R^+, R^-), classifier)$

Benefits over traditional active learning. Our DSM algorithm offers several benefits over traditional active learning. (1) *Better accuracy*: DSM performs predication first using the data space model and if uncertain, then using the classifier. Hence it can provide better accuracy than the classifier alone given the same number of training examples. (2) *Lower bound on accuracy*: DSM also offers a formal lower-bound on F1-score, as described below.

3.3 Lower Bounds of F1-score

With a understanding of how the DSM algorithm works, we now present formal results on the model accuracy achieved by DSM.

Exact Lower Bound. We begin with an exact lower bound of our accuracy measure, the F1-score.

Theorem 3.1 *The three-set metric evaluated on D_{eval} captures a lower bound of the F1-score if* DSM *is evaluated on D_{test}.*

The lower bound of DSM has several features. First, it is an *exact* lower bound throughout the exploration process for any evaluation set D_{eval}. Second, the metric is *monotonic* in the sense that points in the uncertain region D^u can be moved to the positive or negative region later, but not vice versa, and the metric goes to 1 when $D^u = \emptyset$. If the metric is above the desired accuracy threshold at some iteration, it is guaranteed to be greater than the threshold in later iterations, so we can safely stop the exploration. Monotonicity also

enables incremental computation: at iteration $i+1$, we only need to check the points in the uncertain region at iteration i and see if they belong to the positive or negative region of iteration $i+1$.

Approximate Lower Bound. When D_{eval} is too large, we employ a sampling method to reduce the time to evaluate the three-set metric. Let p and q be the true proportions of the positive and negative examples in D_{eval}, i.e., $p = |D^+|/|D_{eval}|$ and $q = |D^-|/|D_{eval}|$. Then the three-set metric is $b = \frac{p}{1-q}$. Let $\hat{p}$ and $\hat{q}$ be the observed proportions of the positive and negative examples in a random draw of n examples from D_{eval}, and let $X_n = \frac{\hat{p}}{1-\hat{q}}$. Our goal is to find the smallest sample size n such that the error of the estimation X_n from the exact three-set metric is less than δ with probability no less than λ. That is, $\Pr(|X_n - b| < \delta) \geq \lambda$.

The following theorem will help us find the lower bound of n.

Theorem 3.2 *$sup_\epsilon \| \Pr(\sqrt{n}|X_n - b| < \epsilon) - \left(2\Phi(\frac{\epsilon(1-q)}{\sqrt{p(1-p-q)}}) - 1\right) \| = O(1/\sqrt{n})$ for any ϵ, where Φ is the cumulative distribution function of the standard Normal distribution.*

With the theorem, we can approximate the sample size such that

$$2\Phi(\frac{\sqrt{n}\delta(1-q)}{\sqrt{p(1-p-q)}}) - 1 \geq \lambda.$$

Since $p(1-p-q)/(1-q)^2 \leq 1/4$, it is sufficient for n to satisfy $2\Phi(2\sqrt{n}\delta) - 1 \geq \lambda$ and therefore $n \geq \left(\Phi^{-1}\left(\frac{\lambda+1}{2}\right)\right)^2/(4\delta^2)$.

3.4 Optimization of Sampling Methods

There are several `subsample` procedures in Algorithm 1. We present their implementation and optimization as follows.

Sampling for creating the evaluation set (OPT1). In line 1 of Algorithm 1, we construct an evaluation set D_{eval} to develop a lower bound of the DSM model. Ideally, we want D_{eval} to be as large as the entire database D. For efficiency, we can only afford to have a memory-resident sample. The analysis in Theorem 3.2 indicates that we can choose a sample of size n from the database, and achieve an approximate lower bound of the F1-score of our DSM algorithm when evaluated on the database. The sample, denoted as $\tilde{D}_{eval}$, will expedite line 10 of Algorithm 1.

For instance, the SDSS database used in our experiments contains 190 million tuples. Denote the true lower bound as b. When $n = 50k$, our approximate lower bound $\hat{b}$ approximates b by $\epsilon \leq .005$ with probability 0.975 or higher. When $n = 1.9$ million, $\hat{b}$ approximates b by $\epsilon \leq .001$ with probability 0.994 or higher.

Sampling for pool-based active learning (OPT2). Algorithm 1 contains two `subsample` procedures for pool-based uncertainty sampling, that is, choosing the most uncertain example from the pool for labeling next. The `subsample` routine in line 17 creates a pool of unlabeled examples from the uncertain partition of the evaluation set, D^u, which is memory-resident. This can be easily implemented using reservoir sampling. The `subsample` routine in line 21, however, creates a pool, from the unlabeled portion of the entire database, which is large and not materialized.

Since sampling from the database at each iteration is costly, we propose to sample the database once before the interactive exploration starts, to create a set called DBmirror, and then use the unlabeled instances in DBmirror, denoted as $\mathcal{U}$, as our pool in line 21. If we use SVM based uncertainty sampling in line 22 with the random top l method [5, 16] (described in Section 2.2), we prove in Proposition 3.3 that we can use $\mathcal{U}$ to replace the pool and avoid subsampling the entire database at each iteration in line 21. Specifically, it guarantees that the probability of finding at least one user-to-label instance that is among the top p% of closest instances to the current boundary in the database, converge to $1-\eta$ as $m = |\text{DBmirror}|$ goes to infinity. For example, with $l = 5000, m = 1.9e+5$, the probability is within $1e$-11 of $1-\eta$ when $p\% = .5\%$, and it is within 0.0023 of $1-\eta$ when $p\% = .1\%$.

Proposition 3.3 (Initial pool for random top sampling) *Let $\mathcal{U}$ be the current unlabeled instances in DBmirror, and B be the current decision boundary. A random sample of size l is drawn from $\mathcal{U}$ and scanned to find the instance closest to B for the user to label, where l is chosen so that*

$$\Pr(\textit{at least one in the } l \textit{ draws is among the top } p\% \textit{ closest to } B \textit{ in } \mathcal{U}) = 1 - (1-p)^l = 1 - \eta.$$

Let A be the event that at least one in the l draws is among the top $p\%$ closest to B in the unlabeled database, $D_{unlabled}$. Since the probability of A depends on the specific instances in $\mathcal{U}$, let $\Pr(A|\mathcal{U})$ denote the probability of A as a function of the random instances in $\mathcal{U}$. Then l chosen this way guarantees that

$$\Pr(A|\mathcal{U}) \xrightarrow{p} 1-\eta, \textit{as } m = |\textit{DBmirror}| \to \infty, \textit{ further}$$

$$\sqrt{m}(\Pr(A|\mathcal{U}) - (1-\eta)) \xrightarrow{d} N(0, l^2 p(1-p)^{2l-1}).$$

4. FACTORIZATION

Although DSM can reduce the user labeling effort and offer better accuracy than traditional active learning, with increased dimensionality the volume of its uncertain region may grow fast and hence degrade its performance. To address this issue, we leverage the property of *conjunctive queries* to factorize a high-dimensional data space into a set of low-dimensional spaces. By running the polytope model in each of the low-dimensional spaces, we can "simulate" DSM in the high-dimensional space with much improved performance. This extension, denoted as DSM$_F$, may require user labels of examples in some subspaces. In particular, if the user label is positive for an example, the label in each subspace is inferred to be positive. However, if the user label is negative for an example, she will be asked to specify the subset of attributes (and the subspaces thereof) that lead to the negative label. Since the user has gone through thinking when deciding the label, asking her to specify a subset of attributes that lead to the negative label can be facilitated through a graphical interface such as in [12].

Factorization for DSC queries. Formally, factorization concerns a user interest query Q defined on an attribute set $\boldsymbol{A}$ of size d, and can be written in the conjunctive form, $Q_1 \wedge \ldots \wedge Q_m$. Each Q_i, $i \in [1 \ldots m]$, uses a subset of attributes $\boldsymbol{A}_i = \{A_{i1}, \cdots, A_{id_i}\}$. The family of attribute sets, $\boldsymbol{A} = (\boldsymbol{A}_1, \cdots, \boldsymbol{A}_m)$, is pairwise disjoint with $d = \sum_{i=1}^m d_i$, and is called the *factorization structure*.

In practice, we can derive the factorization structure from available data in a database. It is a partitioning of the database attributes with two properties: 1) Each attribute can appear in only one partition. 2) If several attributes may be used in the same predicate (e.g., the positional attributes $rowc$-$colc$, or the velocity attributes $rowv$-$colv$ from SDSS), they must be assigned to the same partition. If a query trace is available to show how attributes are used in predicates, e.g., individually or in a pair, we can run a simple algorithm over the query trace: Initially assign each attribute to its own partition. As the query trace is scanned, two partitions are merged if a predicate uses attributes from the two partitions. At the end, all the remaining partitions become the factorization structure $\boldsymbol{A}$. Even if a query trace is not available, it is not unreasonable to assume

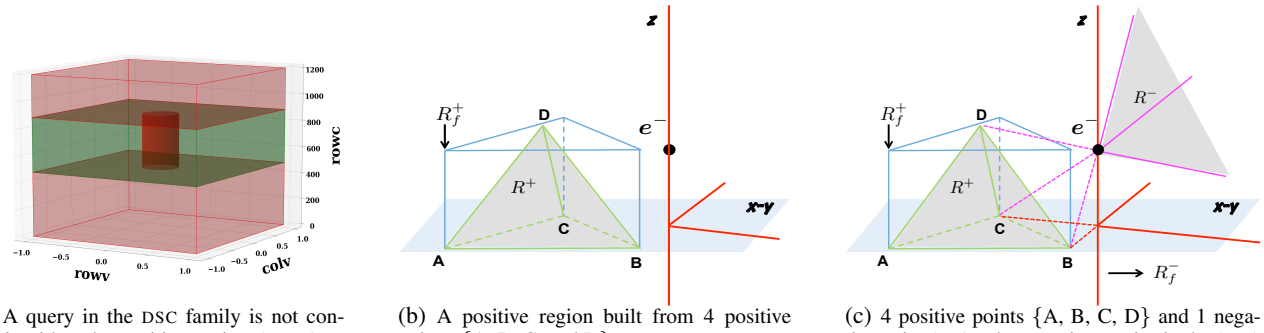

(a) A query in the DSC family is not convex in either the positive region (green) or the negative region (red).

(b) A positive region built from 4 positive points, {A, B, C, and D}

(c) 4 positive points {A, B, C, D} and 1 negative point (e^-), where e^- is negative in the (x-y) subspace and positive in the (z) subspace

Figure 4: Illustration of factorization when 3D space (x-y-z) is factorized into two subspaces (x-y) and (z).

that by working with domain experts, it is possible to extract a reasonable factorization structure that reflects how attributes are used based on their semantics, e.g., the velocity attributes $rowv$-$colv$ are often used in the same predicate.

DSC Queries. We next define a class of user interest queries that DSM$_F$ supports with benefits over active learning: that is, $\forall i = 1, \ldots, m$, either the positive region in the i^{th} subspace, defined as $\{\boldsymbol{x}_i \in \mathbb{R}^{|\boldsymbol{A}_i|} | Q_i(\boldsymbol{x}_i) > 0\}$, is convex (in the $\mathbf{Q}_c^+$ class), or the negative region, $\{\boldsymbol{x}_i \in \mathbb{R}^{|\boldsymbol{A}_i|} | Q_i(\boldsymbol{x}_i) < 0\}$ is convex (in $\mathbf{Q}_c^-$). We call such queries *Decomposable Subspatial Convex* (DSC) queries.

DSC allows us to combine a subspace whose positive region is convex with another subspace whose negative region is convex. However, the global query is **not** necessarily convex in either the positive or negative region. Fig. 4(a) shows an example query, $Q = x^2 + y^2 > 0.2^2 \wedge 480 < z < 885$, which combines the ellipse pattern in Fig. 2(d), whose negative region is convex, with the line pattern in Fig. 2(a), whose positive region is convex. In the 3D space, the negative region (marked in red) is the union of the red cylinder in the middle of the figure and the red rectangles above and below the cylinder, while the positive region (marked in green) is the complement of it. Neither of the positive nor the negative region of Q is convex although it belongs to DSC.

p-DSC Queries. We also support a superset of DSC queries, which requires only some subspaces for which the convex assumption holds. We call this generalization *partial factorization* or p-DSC.

As a special case, if none of the subspaces permits the convexity property, we call such queries *Zero* DSC or 0-DSC.

Polytope model with factorization and DSM$_F$. Given the factorization structure, the polytope model runs in each subspace where the subspatial convexity is deemed true. First, in the i^{th} subspace defined by $\boldsymbol{A}_i$, Q_i's positive and negative regions, denoted as R_i^+ and R_i^-, are built according to Definition 3.1 and 3.2, but based on the "positive" and "negative" labels of projected examples for Q_i, as described above. Then we build the positive and negative regions of Q from the positive and negative regions in the subspaces via the *conjunctive property*:

$$R_f^+ = \times_{i=1}^m R_i^+, \quad R_f^- = \left(\times_{i=1}^m (R_i^-)^c\right)^c \tag{2}$$

where $\times$ denotes the Cartesian product between two sets, and R^c denotes the complement of set R. Then the uncertain region of Q is, $R_f^u = \mathbb{R}^d - R_f^+ - R_f^-$.

Next we formally define the decision function for the polytope model with factorization. In each subspace defined on $\boldsymbol{A}_i$, let $F_{\boldsymbol{A}_i} : \mathbb{R}^{|\boldsymbol{A}_i|} \rightarrow \{-1, 0, 1\}$ be the decision function that divides the subspace into three disjoint regions corresponding to the negative, unknown, and positive regions, respectively. As in (Eq. 1),

$$F_{\boldsymbol{A}_i}(x) = 1 \cdot \mathbb{1}(\boldsymbol{x} \in R_i^+) - 1 \cdot \mathbb{1}(\boldsymbol{x} \in R_i^-). \tag{3}$$

For p-DSC queries, if the subspatial convexity is deemed not true in a subspace, the value of its decision function is a constant zero.

The global decision function for the polytope model with factorization over the entire data space is then

$$F_{\mathcal{D}_f}(\boldsymbol{x}) = \min_{i=1}^m F_{\boldsymbol{A}_i}(\boldsymbol{x}_i) \tag{4}$$

where $\boldsymbol{x} = (\boldsymbol{x}_1, \ldots, \boldsymbol{x}_d)$, and $\boldsymbol{x}_i$ denotes the projection of $\boldsymbol{x}$ on the i^{th} subspace defined by $\boldsymbol{A}_i$.

Finally, consider the dual-space model. Let DSM$_F$ be DSM in §3.2 with the polytope data space model $F_{\mathcal{D}}$ replaced by the polytope model with factorization $F_{\mathcal{D}_f}$. The algorithm for DSM$_F$ modifies Algorithm 1 only in line 9: updateRegion, where we use labeled examples to build the positive and negative regions of Q through factorization, as described in Eq. 2.

Then the dual-space decision function of DSM$_F$, $H : \mathbb{R}^d \rightarrow \{-1, 1\}$, is:

$$H(\boldsymbol{x}) = \begin{cases} F_{\mathcal{D}_f}(\boldsymbol{x}), & F_{\mathcal{D}_f}(\boldsymbol{x}) \neq 0 \\ F_{\mathcal{V}}(\boldsymbol{x}), & \text{otherwise} \end{cases} \tag{5}$$

where $F_{\mathcal{V}}$ is the classification model. H is our final prediction model returned to approximate the user interest query Q, denoted as $H(\boldsymbol{x}) \sim Q(\boldsymbol{x}) \rightarrow \{-1, 1\}$, where $Q(\boldsymbol{x}) = 1$ if the tuple $\boldsymbol{x}$ belongs to the query answer set, and $Q(\boldsymbol{x}) = -1$, otherwise. For 0-DSC queries, DSM$_F$ simply runs traditional active learning.

Illustration. Before presenting the formal results, we illustrate the intuition that factorization allows us to construct the positive and negative regions (R_f^+, R_f^-) as supersets of (R^+, R^-), hence reducing the unknown region and offering better accuracy.

Fig. 4(b) shows four positive points A, B, C, D when the 3D space (x-y-z) is factorized into two subspaces (x-y) and (z). It depicts the positive region R^+ as the pyramid shaded in grey and marked by the green lines. When we factorize R^+ into (x-y) and (z) planes, we have R_{xy}^+ as a triangle marked ABC and R_z^+ as a line segment projected onto z. Then we construct R_f^+ from the triangle and the line segment based on Eq. 2, we obtain a prism marked by the blue lines, which is much bigger than R^+.

Fig. 4(c) shows a negative point e^- and the negative region constructed for it. R^- is a convex cone shaded in grey and bounded by the solid purple rays emitting from e^-. When e^- is projected onto (x-y), it is negative and defines a convex cone R_{xy}^- marked by the two solid red lines in the (x-y) plane. When e^- is projected onto z, it lies in the positive region. According to Eq. 2, the new negative region R_f^- extends the convex cone R_{xy}^- by all possible values of z, resulting in a geometric shape enclosed by the three solid red lines in the figure. Again, the new R_f^- is much larger than R^-.

Formal results. We prove the following results of the polytope model with factorization for both DSC and p-DSC queries.

Proposition 4.1 *All points in the positive region R_f^+ are positive and $R^+ \subseteq R_f^+$ at each iteration of the data exploration process.*

Proposition 4.2 *All points in the negative region R_f^- are negative and $R^- \subseteq R_f^-$ at each iteration of the data exploration process.*

Proposition 4.3 DSM$_F$ *improves the Three-Set Metric, the lower bound of the model accuracy in F1-score, over* DSM.

Proposition 4.1 states that the positive region constructed via factorization is correct and a superset of the positive region that the original DSM offers. The intuition is that building a convex polytope from a small set of positive examples in high-dimensional space grows the positive region slowly. Once we know the conjunctive property, we build such polytopes in subspaces and the cartesian products between these polytopes allow the positive region to grow much faster. Proposition 4.2 makes a similar statement for the negative region. Again given the conjunctive property, if a data example is negative in any subspace, its combination with all possible values in other subspaces belong to the negative region, hence growing the negative region fast. When both the positive and negative regions (R_f^+, R_f^-) are supersets of (R^+, R^-), the uncertain region is reduced and the lower bound of F1-score built from (R_f^+, R_f^-) is higher than that from (R^+, R^-) according to Def. 3.4.

Testing assumptions of DSM$_F$. Factorization replies on two assumptions, which our system will test when a user is performing data exploration online. The first assumption is that we have a correct factorization structure, $\boldsymbol{A} = (\boldsymbol{A}_1, \cdots, \boldsymbol{A}_m)$, for a database derived from its query trace or schema. The second assumption is that user interests take the form a conjunctive query (CQ). In fact, our system offers a simple extension of DSM to handle categorical attributes, which is left to [23] in the interest of space. With this extension, the class of user interest queries is an *extended class of conjunctive queries*, in the form of $P_1 \wedge P_2 \wedge \ldots$, such that either P_i is an individual predicate, or P_i is defined on a categorical attribute A and can take the disjunctive form, $A = 1 \vee A = 2 \vee ...$

Test Procedure. When either the factorization structure or the CQ assumption is wrong, we start to see conflicting examples in a polytope model for a specific subspace, that is, a positive example labeled by the user appears in the negative region or vice versa. Based on this intuition, our system uses the following procedure to test online both assumptions behind DSM$_F$. From the beginning of data exploration, we build two polytope models for each subspace, one under the assumption that the positive region is convex, $\mathbf{Q}_c^+$, the other under the assumption that the negative region is convex, $\mathbf{Q}_c^-$. Over iterations, we count the number of conflicting examples of these two polytope models, and use a threshold, T, to turn off a polytope model if its count exceeds T. If both polytope models remain active in a given iteration, the one with the smaller count will be used; in the case of a tie, the model for $\mathbf{Q}_c^+$ will be used as more query patterns belong to this class. When both polytope models for a subspace are turned off, we use partial factorization until they are turned off for all subspaces, when we resort to the classifier. Finally, the test procedure also allows DSM$_F$ to handle a certain amount of inconsistent (noisy) user labeling by adjusting the threshold T, the number of conflicting examples that can be tolerated by each polytope model.

5. ONLINE FEATURE SELECTION

The user exploration task may start with more attributes than those included in the final learned model (user interest query). The attributes that are not included in the final model are noise in data exploration and cause slow convergence of the model. To remove such noisy attributes, we employ both offline dimensionality reduction on the database and online feature selection techniques.

We examined a range of dimension reduction methods including PCA for offline compression, and Random forests (RF) and Gradient boosting regression trees (GBRT) for online feature selection. Since these are standard methods, we leave their description and evaluation to Appendix B.2 in [23]. Overall we found that GBRT works best for reducing the dimensions needed for the user interest model. We next outline how GBRT is used for online feature selection in our work[3]. In each iteration of data exploration, we first feed all labeled examples to the GBRT learner, and ask the learner to return the top-k features that are deemed most important in learning. Then we build the classifier using these features and select the next example for labeling. We repeat the two steps in each iteration until the choice of the top-k features has stabilized (to be formalized shortly). Then we build the full DSM$_F$ model until it converges. However, we observe two limitations of this approach:

Unbalanced training data. GBRT is very sensitive to unbalanced classes, that is, when the training data is dominated by the negative examples. This is common in data exploration because the true user interest is often a highly selective query. We draw upon two insights in this work to mitigate the imbalance problem. First, when applicable, our DSM$_F$ algorithm already maintains a list of positive examples from the evaluation set and we can add them to make the training data balanced. Second, before DSM$_F$ accumulates enough positive examples, we can also boost GBRT using synthetic positive data: if the user interest has a convex shape, as long as there are two positive examples, we can draw points from the line that connects these two examples, and treat these points as synthetic positive examples to balance the training data.

How many features to select? Another issue is that we do not know how many features to select, or the exact value of top-k. The user does not offer this information a priori. Choosing the right value of k is nontrivial because GBRT may not have high confidence for selecting the correct features in earlier iterations: in some iterations it ranks the correct features above others, but in the next iteration it may change its ranking.

To formalize the notion of confidence, we utilize the feature importance scores provided by GBRT. GBRT is a linear combination of decision tree base-learners, where each decision tree intrinsically selects features for splitting nodes. For each decision tree, the importance score of a feature is computed as weighted sum of impurity decreases for all the nodes where the feature is used [6]. Then this score is averaged over all trees. Given feature importance scores, we propose two strategies to characterize "sufficient confidence" of GBRT for feature selection.

Proportion of nonroot trees: The intuition is that all decision trees must be weak learners and hence find some features useful in distinguishing the positive class from the negative class. Based on this intuition, we wait until the iteration where all trees become nonroot trees, hence likely to be weak learners. Then we believe that the confidence of GBRT has reached a sufficient level.

Entropy of Importance Scores (EIS): The next intuition is that we prefer to have a lower entropy of the importance scores across all the features. That is, the distribution of importance scores departs from a uniform distribution and becomes concentrated. Based on this, our second strategy is to wait until EIS has dropped significantly below the expected entropy of uniform importance scores, i.e., the importance scores of some features really stand out. Then we think that the confidence of GBRT has been sufficient.

[3]Since *feature selection* is the standard term in the literature, we use "features" and "attributes" interchangeably in this context.

Table 1: Query templates instantiated with different selectivity values

Query template
Q1 (rectangle): $rowc \in [a_1, a_2] \wedge colc \in [b_1, b_2]$
Q2 (ellipse): $((rowc - a_1)/b_1)^2 + ((colc - a_2)/b_2)^2 < c^2$
Q3 (rectangle): $ra \in [a_1, a_2] \wedge dec \in [b_1, b_2]$
Q4 (outside a circle): $rowv^2 + colv^2 > c^2$
Q5: 4D queries combining two queries from Q1-Q4
Q6: 6D queries combining three from Q1-Q4
Q7: 6D-11D queries with 4-9 irrelevant attributes
Q8: 4D, $(x_1 > a + b \cdot x_2) \wedge (x_3 + c \cdot \log_{10} x_4^2 < d)$

Adaptive Feature Selection: We next devise adaptive strategies to decide top-k features, depending on whether the current iteration has reached the point of sufficient confidence for feature selection, based on any of the above strategies. Before reaching this point, we perform conservative feature filtering to accommodate the uncertainty of GBRT; we select top-k features that account for 50% of the total feature importance scores. After GBRT reaches the point of sufficient confidence, we perform aggressive feature selection by scanning the ranked list of feature importance scores and choosing the top-k features such that the k^{th} feature and the $k + 1^{th}$ feature have the largest gap in the ranked list. When GBRT chooses the same top-k features for 10 iterations, we consider the choice of relevant features stable and use them to build DSM$_F$.

6. EXPERIMENTAL EVALUATION

We implemented all of our proposed techniques in a Java-based prototype for data exploration, which connects to a PostgreSQL database. In this section, we evaluate our techniques and compare to recent active learning algorithms [5, 16], active search [17], and explore-by-example systems, Aide [13, 14] and LifeJoin [10].

Datasets: Our evaluation used two datasets. (1) SDSS (190 million tuples) contains the "PhotoObjAll" table with 510 attributes. By default, we used 1% sample (1.9 million tuples, 4.9GB) to create an evaluation set for DSM and for pool-based uncertainty sampling – our formal results in §3.4 allowed us to use the 1% sample for data exploration, yet with bounded difference of $\epsilon \leq .001$ from the accuracy achieved over the full database with probability $\geq$0.994. (2) Car database (5622 tuples): this small dataset is used for our user study because it is more intuitive for users to perform explorative analytics. We defer a detailed discussion to §6.4.

User Interest Queries: We extracted a set of query templates from the SDSS query release [40] to represent user interests. They allow us to run *simulations* of user exploration sessions as in [13,14]: We precompute the answer set of each query as the proxy of the user. We then run a data exploration session as described in Algorithm 1; in each iteration when DSM chooses a new example for labeling, the simulator consults the proxy to get a positive or negative label.

Our experiments used 8 templates as shown in Table 1. Each template is instantiated with different constants to vary query selectivity in [0.01%, 10%]. Our system does **not** need to know these templates in advance, but rather learns their decision boundaries on the fly. In particular, Q1-Q3 represent patterns that are convex in the positive region ($\mathbf{Q}_c^+$). Q4 retrieves tuples outside a circle, hence in the $\mathbf{Q}_c^-$ class. Q5-Q7 combine these attributes, optionally with irrelevant attributes, for scalability tests. Q8 includes a predicate on $x1$ and x_2 that belongs to $\mathbf{Q}_c^+$, and a log predicate on x_3 and x_4 that belongs to $\mathbf{Q}_c^-$ if $x_4 > 0$ or is non-convex if $x_4 \in \mathbb{R}$.

6.1 Dual-Space Algorithm with Factorization

We evaluate our Dual-Space Model (DSM) and compare it to two ML techniques: (i) Active Learning (AL) runs uncertainty sampling [5, 16] to obtain labeled examples for building a classifier, which is the version space part of DSM. We run AL with an SVM or a standard kNN classifier (denoted as kNN$^+$). (ii) Active Search (AS) [17] also follows an iterative procedure of asking the user to label an example and training a new model to guide the selection of the next example, but uses a strategy to maximize the number of positive examples in the set of selected examples, not classification accuracy. It uses a special variant of kNN classifier to enable optimization, denoted as kNN$^-$. We also did hyper-parameter tuning to achieve best accuracy of AS under per-iteration time and memory constraints. More details are given in [23]. All tests were run up to 500 labeled examples or when the lower bound of F1-score reaches 99%. In all plots, the x-axis is the number of labeled examples.

Expt 1 (2D queries): We run 2D queries from templates Q1 to Q4. Since the results show similar trends, we show the F1-score, lower bound, and time measurement for Q3 (1%) in Fig. 5(a)-5(d).

Regarding accuracy, we see a major trend that DSM outperforms AL, and AL outperforms AS. Details are as follows. (1) A factor that affects performance is the data distribution around the decision boundary B of the user interest query. If B falls into a sparse data region, finding the separation between the positive and negative classes is relatively easy for DSM and AL. Fig. 5(a) shows that for Q3 whose decision boundary is in a sparse region, DSM and AL-SVM converge within 10 labeled examples. However, AS performs poorly, with F1-score less than 20%. The reason is that AS compromises recall by searching close to existing positive examples. In contrast, DSM and AL aims to maximize classification accuracy by sampling the most uncertain region of the model, e.g., close to the decision boundary, hence offering better F1-score. (2) If B falls into a dense data region, learning an approximate $\tilde{B}$ that can accurately divide all unlabeled data points requires more labeled examples. To reach 95% accuracy, DSM requires 100 labeled examples for Q3 and 90 examples on average for Q1-Q4. AL works better with the SVM than the kNN classifier, but even AL-SVM cannot reach 95% for Q3 or most other workloads. Finally, AS performs much worse than AL-KNN$^+$ while both use a kNN classifier.

In addition, DSM further provides a lower bound in F1-score, which is not available with AL or AS. Fig. 5(c) shows that the lower bound is quite close to the true F1-score.

Regarding the time cost, DSM's performance depends on the sampling method. Recall from Algorithm 1 that with probability γ, it samples from the unknown partition of the polytope model, D^u; otherwise, it does so from a subsample of the unlabeled examples in the database, $D_{unlabeled}$. γ=0 leads to high time costs because the examples retrieved from $D_{unlabeled}$ may repeatedly fall in the positive or negative region of the polytope model, wasting resources with no new information. γ=1 and γ=0.5 significantly reduce the time cost, with γ=0.5 offering slightly better accuracy due to balanced sampling. However, both settings exhibit a spike in time cost in the early phase, which is the time to build the polytope model the first time by scanning the entire evaluation set. Finally, we improve γ=0.5 with the optimization (OPT1) from §3.4, where we start with a smaller evaluation set to avoid the initial spike, but later switch to a larger evaluation set once its polytope model is built completely in the background. This optimization keeps the time cost per iteration within a second and will be used as the default algorithm.

Expt 2 (4D-6D queries): We next show results of 4D-6D queries in dense regions as they present harder workloads. The main observations from Fig. 5(e)-5(i) are: (1) Without factorization, DSM performs similarly to AL because the polytope model is dominated by the uncertain region, hence not effective. With factorization, DSM$_F$ dramatically shrinks the uncertain region, and improves the lower bound and the actual F1-score. Interestingly, DSM$_F$ performs even better for a lower selectivity (0.01%) of Q4 than the 1% version,

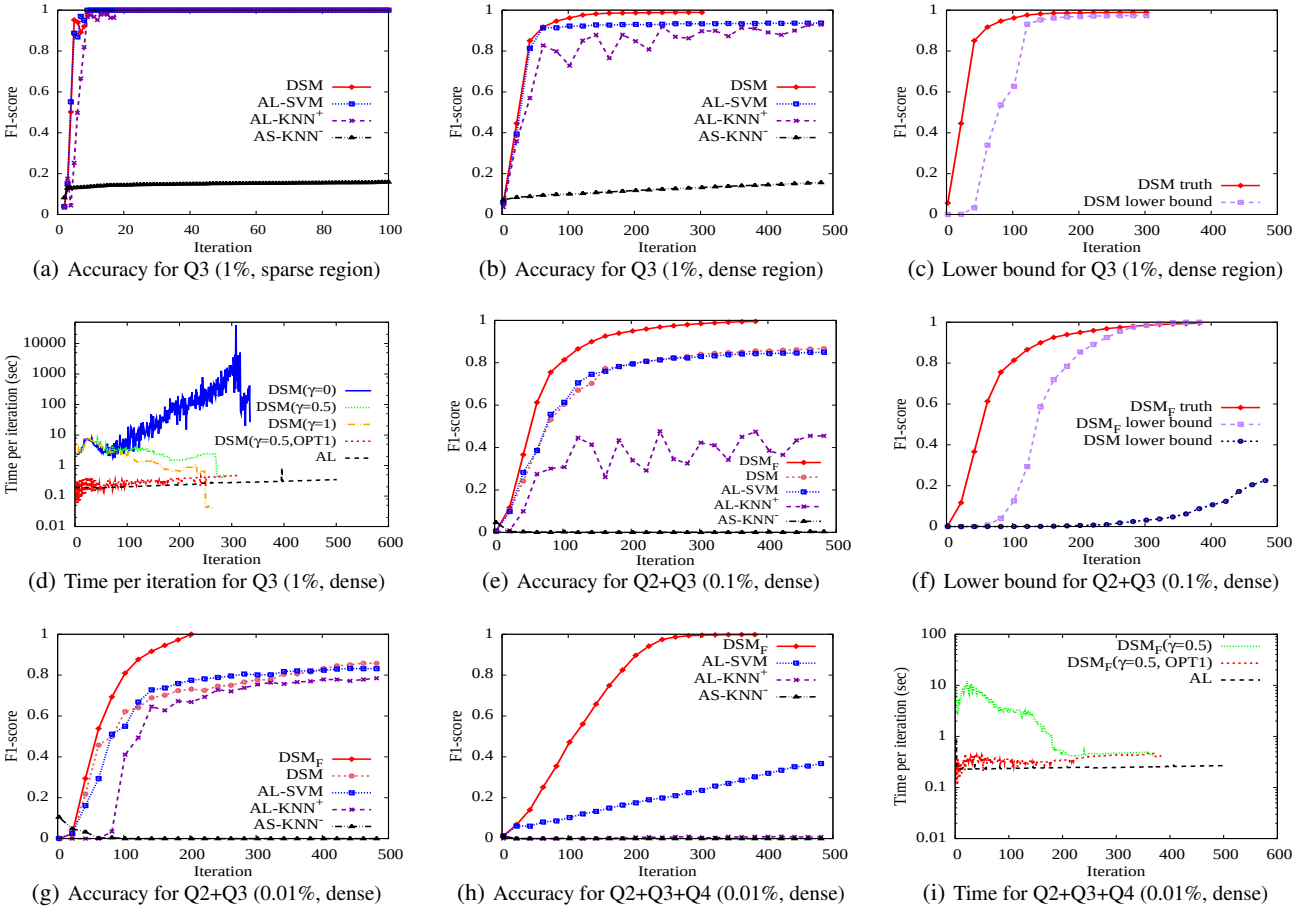

(a) Accuracy for Q3 (1%, sparse region) (b) Accuracy for Q3 (1%, dense region) (c) Lower bound for Q3 (1%, dense region)

(d) Time per iteration for Q3 (1%, dense) (e) Accuracy for Q2+Q3 (0.1%, dense) (f) Lower bound for Q2+Q3 (0.1%, dense)

(g) Accuracy for Q2+Q3 (0.01%, dense) (h) Accuracy for Q2+Q3+Q4 (0.01%, dense) (i) Time for Q2+Q3+Q4 (0.01%, dense)

Figure 5: DSM with factorization for 2D, 4D, and 6D user interest queries, compared against Active Learning (AL) and Active Search (AS) algorithms

as shown in Fig. 5(e) and Fig. 5(g). This can be explained by the diagrams in Fig. 4. When the query region becomes smaller, more examples are negative and for each such example x, we get more subspaces where x's projection falls in the negative region. Then the overall negative region built from these subspaces grows fast, hence reducing the size of the uncertain region. (2) Consistently, DSM outperforms AL, which further outperforms AS. Fig. 5(h) shows that for the 6D query, DSM$_F$ reaches 95% with 240 examples, AL-SVM cannot reach 40% with 500 labeled examples, and AS has F-score close to 0. (3) DSM$_F$ can keep the time per iteration within 1-2 seconds, as shown in Fig. 5(i) for the 6D query.

Expt 3 (partial factorization): We next generate two queries from Q8 with 7.8% selectivity (based on the constants used in SDSS). Q8.v_1 is in the DSC family because its positive region is convex in the ($x1$, x_2) subspace, and its negative region is convex in (x_3, x_4). Q8.v_2 is in the p-DSC family because it is non-convex in (x_3, x_4). Hence, DSM supports Q8.v_2 with partial factorization (§4). Fig. 6(a) shows that DSM$_F$ works better for the DSC query than p-DSC query, as expected, but even partial factorization works much better than AL, which does not reach 60% after 500 labeled examples, and AS, which cannot achieve more than 5% accuracy.

6.2 Online Feature Selection

Expt 4 (Feature selection for 6D-11D queries): We now evaluate the optimizations proposed for GBRT as an online feature selection method in §5. To do so, we use the query template Q7. Since the major results are similar, below we report results by extending Q2 with 4 irrelevant attributes (making it a 6D query) or with 9 irrelevant attributes (making the query 11D). Fig. 6(b) shows the F1-score. Without feature selection, the F1-score is 0 for these queries. Feature selection improves the F1-score to above 80% for all of them. As stated earlier, GBRT is sensitive to the selectivity and hence the combination of high dimensionality (11D) and low selectivity (0.1%) represents the hardest workload among the three.

Fig. 6(c) further shows the effect of optimizations in §5 for the hardest 11D query. No feature selection ("nofs") has 0 accuracy. If we manually feed the correct number of features, balancing the skewed training data using the convex property based on 1 initial positive example ("man-bfs-1pos") cannot improve much from the unbalanced case ("man-ufs-1pos") for this hard query. However, doing so with two initial positive examples makes the optimization more effective ("man-bfs-2pos"). When we use our strategy to adaptive select the top-k relevant features ("ada-bfs-2pos"), we gain even better performance than the manual selection strategy.

6.3 Comparison to Alternative Systems

We next compare our system to two state-of-the-art explore-by-example systems: 1) LifeJoin [10] uses SVM for classification and active learning for seeking the next example for labeling. But it differs in the SVM implementation from our work. We implemented LifeJoin techniques as additional methods in our system. 2) Aide [13, 14] uses decision trees as the classification model and customized methods for seeking the next example for labeling. We obtained the source code from the authors. When comparing these systems, we exclude the overhead to find the first positive example as these systems use different methods / assumptions to find them.

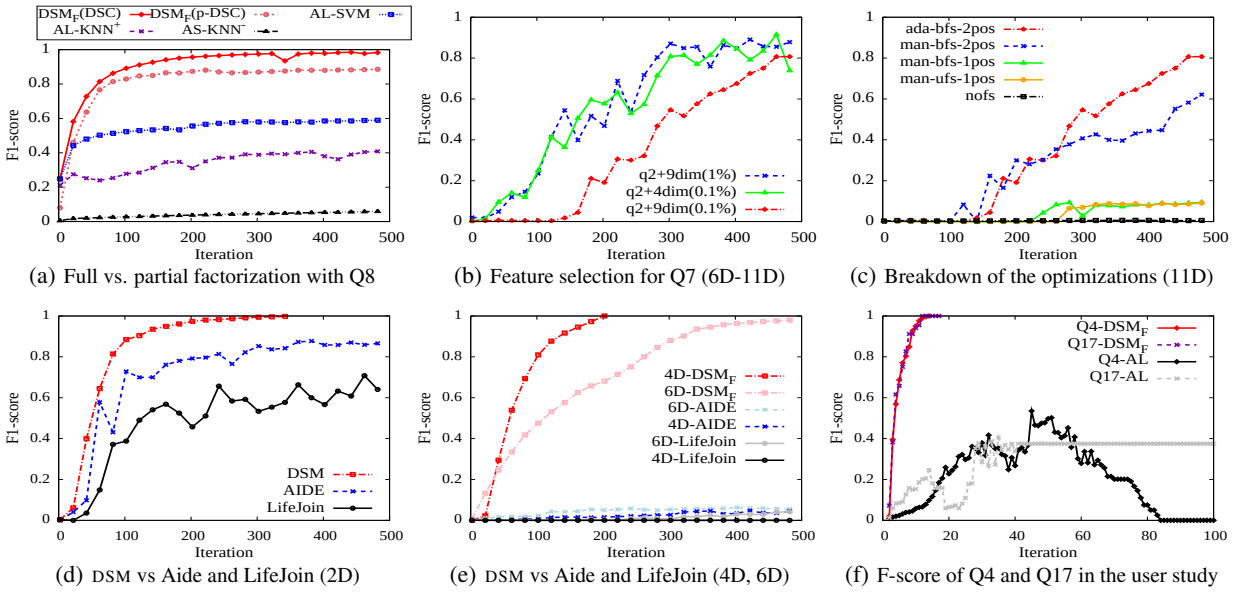

(a) Full vs. partial factorization with Q8 (b) Feature selection for Q7 (6D-11D) (c) Breakdown of the optimizations (11D)

(d) DSM vs Aide and LifeJoin (2D) (e) DSM vs Aide and LifeJoin (4D, 6D) (f) F-score of Q4 and Q17 in the user study

Figure 6: Results for partial factorization, feature selection, and comparison to Aide and LifeJoin systems, and the user study.

Expt 5: F1-score is reported in Fig. 6(d) for a 2D query, and in Fig. 6(e) for 4D and 6D queries. (1) For the 2D query, our system outperforms Aide, which further outperforms LifeJoin. Overall, LifeJoin is significantly worse in accuracy. (2) For the 4D query, Aide and LifeJoin drop to below 10% in accuracy, while our system achieves 99% within 200 iterations. For the 6D query, again Aide and LifeJoin fail to work. This observation remains for any query that we tried beyond 2D. This is due to the combination of low selectivity and high dimensionality in data exploration. Additional analysis of these systems is available in [23].

6.4 User Study using a Car Database

We conducted a user study by building a car database[4]. The database includes 5622 vehicles with 27 attributes such as the model, year, length, height, engine power, and retail price. Additional details on the database are given in Appendix C.4 of [23]. Our study has two objectives: (1) build a query trace to understand the characteristics of data exploration tasks in this domain; (2) use this trace as the ground truth of user interests to evaluate our system.

To develop the query trace, we designed task scenarios with different price constraints and usage patterns, e.g., buying a car for everyday city commute, outdoor sports, an elderly in the family, or a small business. The 18 users in our study belong to two groups: the first 11 users are CS professors and graduate students, while the rest of 7 are non-technical people. We asked each user to find all the cars that meet the requirements of the assigned task so that he can provide a recommendation service to customers who belong to the given scenario. Each user proceeds in three phases: 1) Review the schema: Since this is a familiar domain, most users can understand the schema quickly. 2) Initial exploration: We next show sample data to help the user understand the data and materialize his preference. We also ask the user to come up with the first positive example via (a) naming a car that he already has in mind, or (b) reviewing a sample set pre-computed for the given task based on the price constraints, body type, year, etc., and finding one that appears relevant. Two users chose option (a) while the others chose option (b). 3) Iterative manual exploration: In the third phase, the user is asked to specify his interest precisely by (a) sending a SQL query to the database[5]; (b) reviewing a subset of the returned tuples; (c) going back to revise the query. The steps are repeated until the user is satisfied with all returned tuples of the final query.

First, we verify the observations that motivated this work. The selectivities of all 18 queries are in the range of [0.2%, 0.9%]. They contain 117 predicates in total: 70 of them are defined on numerical attributes and are all convex in the positive region. The rest 47 use categorical attributes, for which the notion of convexity does not apply. All the queries are conjunctive; the only disjunction is applied to the categorical attributes.

Second, we evaluate our system by running simulations using these queries as the true user interest. While the queries involve 4 to 10 attributes, the classifier requires categorical attributes to be transformed using one-hot encoding, resulting in 4 to 418 features used by DSM. Table 5 shows in the "DSM" column family that DSM_F achieve 99% for all queries, with a median of 10 labeled examples, despite the high-dimensionality. In contrast, the users manually wrote a series of queries, with a median of 12, and reviewed many tuples, with a median of 98. The results obtained from two user groups are largely consistent with each other, with only a small difference that non-technical people tend to specify simpler queries, hence easier for DSM to learn. Note that the initial cost of finding the first positive example, with a median of 10 tuples, can be added fairly to both exploration modes.

Third, the study verified our performance gains over active learning (AL), which cannot reach 95% accuracy for most queries within 100 iterations and for 80% has a median of 29 labeled examples. Here, even though the decision boundary is often in a sparse region, high dimensionality makes AL degrade performance. Fig. 6(f) shows major difference between DSM and AL for Q4 and Q17, verifying the benefits of the polytope model and factorization.

Fourth, to test the robustness of DSM we run it with noisy user labels as described in §4. Any polytope model that has exceeded T=2 conflicting examples will be turned off, leading to partial factorization. To inject noisy labels, our intuition is that they are more likely to occur close to the boundary of the true pattern. 1) *Noise model*: we use a *Gaussian* noise model where a new example gets a wrong label with a probability that depends on its distance to the

[4]The content is extracted from http://www.teoalida.com/

[5]For the 7 non-techncial people, we offered help to translate their requirements to SQL but otherwise did not influence the users in data exploration.

Table 2: Results of the car database using Manual Exploration, DSM, Active Learning (AL). # A shows the number of attributes used in the user interest and # F shows the number of features (with onehot encoding) after transforming all categorical attributes for use by the classifier. For manual exploration, T_2 shows the number of tuples reviewed in initial exploration (the 2nd phase) for the user to find the first positive example; and T_3 shows those reviewed in iterative exploration (3rd phase). For DSM and AL, the algorithm marked by '-' never reached the desired accuracy within 100 iterations.

Q		# A	# F	Manual Exploration			AL			DSM			DSM: 5 noise free			DSM: 10 noise free			AL: 10 noise free		
				T_2	T_3	#SQL	0.8	0.95	0.99	0.8	0.95	0.99	0.8	0.95	0.99	0.8	0.95	0.99	0.8	0.95	0.99
Q1	**Min**	4	12	0	35	8	8	9	9	4	4	5	4	4	5	4	4	5	8	9	9
$\sim$	**Max**	8	418	18	412	49	-	-	-	14	23	26	-	-	-	14	-	-	-	-	-
Q11	**Mdn**	6	35	11	104	16	29	42	-	7	10	13	7	13	-	7	10	13	35	-	-
Q12	**Min**	4	4	0	50	4	9	15	15	3	5	6	3	5	6	3	5	6	9	16	-
$\sim$	**Max**	10	51	24	260	15	-	-	-	7	11	12	-	-	-	7	11	12	-	-	-
Q18	**Mdn**	6	24	4	91	10	28	-	-	6	6	9	6	6	-	6	6	9	48	-	-
Global	**Mdn**	**6**	**30**	**10**	**98**	**12**	**29**	**-**	**-**	**6**	**9**	**10**	**6**	**11**	**-**	**6**	**9**	**10**	**36**	**-**	**-**

true boundary, i.e., the probability that its distance to the boundary of a perfect SVM classifier (with the margin size δ) is less than a sample from a Gaussian function with u=0 and $\sigma = \delta/2$. 2) *Non-uniform user behaviors*: we assume the first s (=5 or 10) examples to be noise free because they are drawn from the broad data space, hence likely to be far from from the true boundary, and the user tends to be more patient at the beginning. The last 9 columns of Table 5 show DSM and AL under noisy labels. DSM reaches 95% accuracy with a median of 11 labeled examples including 5 noise-free initial examples, while AL requires 36 labeled examples with 10 noise-free examples to achieve 80%. Out of the 105 subspatial polytope models built for 18 queries, 14% were turned off in the case of 5 noise-free initial examples and 6% were turned off in the case of 10 noise-free examples. Partial factorization still outperforms AL for noisy labels due to fast convergence.

7. RELATED WORK

Data Exploration. *Faceted search* iteratively recommends query attributes for drilling down into the database, but the user is often asked to provide attribute values until the desired tuple(s) are returned [27, 35, 36] or offer an "interestingness" measure and its threshold [11]. Semantic windows [26] are pre-defined multidimensional predicates that a user can explore. These methods are different from our active learning based approach. Recent work also supports time series data [33] or avoids false discoveries of statistical patterns [46] during interactive data exploration. Finding best database objects based on user preferences [42] assumes a numeric weight per database attribute, which is different from the active learning approach to discover the user interest on the fly.

Query by Example is a specific framework for data exploration. Earlier work on QBE focused on a visualization front-end that aims to minimize the user effort to learn the SQL syntax [24, 34]. Recent work [32] proposes exemplar queries which treat a *query* as a sample from the desired result set and retrieve other tuples based on similarity metrics, but for graph data only. The work [38] considers data warehouses with complex schemas and aims to learn the minimal project-join queries from a few example tuples efficiently. It does not consider selection with complex predicates, which is the main focus of our work. The work [25] helps users construct join queries for exploring relational databases, and [29] does so by asking the user to determine whether a given output table is the result of her intended query on a given input database.

Query formulation has been surveyed in [9]. The closest to our work is LifeJoin [10], which we compared in Section 6.3. Query By Output (QBO) [44] takes the output of one query on a database, and constructs another query such that running these two queries on the database are instance-equivalent. Dataplay [2] provides a GUI for users to directly construct and manipulate query trees. It assumes that the user can specify the value assignments used in his intended query, and learns conjunctions of quantified Horn expressions (with if-then semantics) over nested relations [1].

Active Learning. Tong and Koller [43] provide a theoretical motivation on selecting new examples using the notion of a version space, but with unknown convergence speed. Related to our work is a lower bound on the probability of misclassification error on the unlabeled training set [7]. However, it relies on user labeling of an additional sample from the unlabeled pool, which is not required in our work. Recent papers [15, 19–21] offere probabilistic bounds for the classification error and sample complexity. Our work differs in that we focus on F1-score, which suits selective user interest queries (imbalanced classes in classification).

Most learning theory makes no assumptions on convex data/class distributions [22]. Clustering techniques can assume that data is clustered in convex sets [22], but address a different problem from ours. In Active Learning, convexity assumptions occur in the Version Space [4, 43], which is the set of classifiers consistent with training data. DSM can embrace any classifier developed through the version space, but also includes the new polytope model.

Active Search. Active search [17, 31, 45] aims to maximize the number of positive examples discovered, called the *Target Set Accuracy*, within a limited budget of user labeling effort. In comparison, our work aims to maximize the *F1-score* of the model learned to approximate the true user interest. We reported the performance difference from [17] in the previous section. The works [31,45] use a kernel function to measure similarity of items in order to maximize the utility of a set of selected items. Such kernel methods have the smoothness requirement, i.e., similar items have similar utility values, and require training data to tune the kernel for each use case (user interest), which do not suit our problem setting.

8. CONCLUSION AND FUTURE WORK

In this paper we presented new algorithms for interactive data exploration in the active learning framework, which leverage the subspatial convex and conjunctive properties of database queries to overcome the slow convergence of active learning. Our results show that our DSM algorithm significantly outperforms active learning [5,16], active search [17], and existing explore-by-example systems, Aide [13, 14] and LifeJoin [10], in accuracy and convergence speed, while maintaining the per-iteration time within 1-2 seconds.

In future work, we will address inconsistent labeling by extending our DSM model to a probabilistic model, extend query patterns to multiple disjoint areas using exploration versus exploitation, and leverage data properties to further improve accuracy, We will also explore database optimizations such as materialized views and multi-query optimization to improve efficiency.

9. REFERENCES

[1] A. Abouzied, D. Angluin, C. H. Papadimitriou, J. M. Hellerstein, and A. Silberschatz. Learning and verifying quantified boolean queries by example. In *Symposium on Principles of Database Systems (PODS)*, 2013.

[2] A. Abouzied, J. M. Hellerstein, and A. Silberschatz. Playful query specification with dataplay. *Proc. VLDB Endow.*, 5(12):1938–1941, Aug. 2012.

[3] C. B. Barber, D. P. Dobkin, and H. Huhdanpaa. The quickhull algorithm for convex hulls. *ACM Trans. Math. Softw.*, 22(4):469–483, Dec. 1996.

[4] K. Bellare, S. Iyengar, A. Parameswaran, and V. Rastogi. Active sampling for entity matching with guarantees. *ACM Trans. Knowl. Discov. Data*, 7(3):12:1–12:24, Sept. 2013.

[5] A. Bordes, S. Ertekin, J. Weston, and L. Bottou. Fast kernel classifiers with online and active learning. *J. Mach. Learn. Res.*, 6:1579–1619, Dec. 2005.

[6] L. Breiman. Random forests. *Machine learning*, 45(1):5–32, 2001.

[7] C. Campbell, N. Cristianini, and A. J. Smola. Query learning with large margin classifiers. In *Proceedings of the Seventeenth International Conference on Machine Learning*, ICML '00, pages 111–118, San Francisco, CA, USA, 2000. Morgan Kaufmann Publishers Inc.

[8] G. Casella and R. L. Berger. *Statistical Inference*. Cengage Learning, 2001.

[9] A. Cheung and A. Solar-Lezama. Computer-assisted query formulation. *Found. Trends Program. Lang.*, 3(1):1–94, June 2016.

[10] A. Cheung, A. Solar-Lezama, and S. Madden. Using program synthesis for social recommendations. In *Proceedings of the 21st ACM International Conference on Information and Knowledge Management*, CIKM '12, pages 1732–1736, New York, NY, USA, 2012. ACM.

[11] D. Dash, J. Rao, N. Megiddo, A. Ailamaki, and G. Lohman. Dynamic faceted search for discovery-driven analysis. In *CIKM*, 2008.

[12] Y. Diao, K. Dimitriadou, Z. Li, W. Liu, O. Papaemmanouil, K. Peng, and L. Peng. AIDE: an automatic user navigation system for interactive data exploration. *PVLDB*, 8(12):1964–1967, 2015.

[13] K. Dimitriadou, O. Papaemmanouil, and Y. Diao. Explore-by-example: an automatic query steering framework for interactive data exploration. In *SIGMOD Conference*, pages 517–528, 2014.

[14] K. Dimitriadou, O. Papaemmanouil, and Y. Diao. AIDE: an active learning-based approach for interactive data exploration. *IEEE Transactions on Knowledge and Data Engineering (TKDE)*, 2016. Accepted for publication.

[15] R. El-Yaniv and Y. Wiener. Active learning via perfect selective classification. *J. Mach. Learn. Res.*, 13(1):255–279, Feb. 2012.

[16] S. Ertekin, J. Huang, L. Bottou, and L. Giles. Learning on the border: Active learning in imbalanced data classification. In *Proceedings of the Sixteenth ACM Conference on Conference on Information and Knowledge Management*, CIKM '07, pages 127–136, New York, NY, USA, 2007. ACM.

[17] R. Garnett, Y. Krishnamurthy, X. Xiong, J. G. Schneider, and R. P. Mann. Bayesian optimal active search and surveying. In *Proceedings of the 29th International Conference on Machine Learning, ICML 2012, Edinburgh, Scotland, UK, June 26 - July 1, 2012*, 2012.

[18] B. Grünbaum. Convex polytopes. In *Convex Polytopes*. Springer-Verlag New York, 2 edition, 2003.

[19] S. Hanneke. Rates of convergence in active learning. *Ann. Statist.*, 39(1):333–361, 02 2011.

[20] S. Hanneke. Theory of disagreement-based active learning. *Found. Trends Mach. Learn.*, 7(2-3):131–309, June 2014.

[21] S. Hanneke. Refined error bounds for several learning algorithms. *J. Mach. Learn. Res.*, 17(1):4667–4721, Jan. 2016.

[22] T. Hastie, R. Tibshirani, and J. Friedman. *The Elements of Statistical Learning*. Springer, 2001.

[23] E. Huang, L. Peng, L. D. Palma, A. Abdelkafi, A. Liu, and Y. Diao. Optimization for active learning-based interactive database exploration. Technical report, 2018. `http://claro.cs.umass.edu/pubs/aide2018.pdf`.

[24] B. E. Jacobs and C. A. Walczak. A Generalized Query-by-Example Data Manipulation Language Based on Database Logic. *IEEE Transactions on Software Engineering*, 9(1):40–57, 1983.

[25] M. Kahng, S. B. Navathe, J. T. Stasko, and D. H. P. Chau. Interactive browsing and navigation in relational databases. *Proc. VLDB Endow.*, 9(12):1017–1028, Aug. 2016.

[26] A. Kalinin, U. Cetintemel, and S. Zdonik. Interactive data exploration using semantic windows. In *Proceedings of the 2014 ACM SIGMOD International Conference on Management of Data*, SIGMOD '14, pages 505–516, New York, NY, USA, 2014. ACM.

[27] N. Kamat, P. Jayachandran, K. Tunga, and A. Nandi. Distributed Interactive Cube Exploration. In *ICDE*, 2014.

[28] S. R. Lay. *Convex Sets and Their Applications*. Dover Publications, 2007.

[29] H. Li, C.-Y. Chan, and D. Maier. Query from examples: An iterative, data-driven approach to query construction. *Proc. VLDB Endow.*, 8(13):2158–2169, Sept. 2015.

[30] W. Liu, Y. Diao, and A. Liu. An analysis of query-agnostic sampling for interactive data exploration. Technical report, University of Massachusetts Amherst, 2016. Technical report UM-CS-2016-003.

[31] Y. Ma, R. Garnett, and J. G. Schneider. Σ-optimality for active learning on gaussian random fields. In *Advances in Neural Information Processing Systems 26: 27th Annual Conference on Neural Information Processing Systems 2013. Proceedings of a meeting held December 5-8, 2013, Lake Tahoe, Nevada, United States.*, pages 2751–2759, 2013.

[32] D. Mottin, M. Lissandrini, Y. Velegrakis, and T. Palpanas. Exemplar queries: Give me an example of what you need. *Proc. VLDB Endow.*, 7(5):365–376, Jan. 2014.

[33] R. Neamtu, R. Ahsan, C. Lovering, C. Nguyen, E. A. Rundensteiner, and G. N. Sárközy. Interactive time series analytics powered by ONEX. In *Proceedings of the 2017 ACM International Conference on Management of Data, SIGMOD Conference 2017, Chicago, IL, USA, May 14-19, 2017*, pages 1595–1598, 2017.

[34] G. Özsoyoglu and H. Wang. Example-Based Graphical Database Query Languages. *Computer*, 26(5):25–38, 1993.

[35] S. B. Roy, H. Wang, G. Das, U. Nambiar, and M. Mohania. Minimum-effort driven dynamic faceted search in structured databases. In *Proceedings of the 17th ACM Conference on Information and Knowledge Management (CIKM)*, 2008.

[36] S. B. Roy, H. Wang, U. Nambiar, G. Das, and M. Mohania. Dynacet: Building dynamic faceted search systems over

databases. In *International Conference on Data Engineering (ICDE)*, 2009.

[37] B. Settles. *Active Learning*. Synthesis Lectures on Artificial Intelligence and Machine Learning. Morgan Claypool Publishers, 2016.

[38] Y. Shen, K. Chakrabarti, S. Chaudhuri, B. Ding, and L. Novik. Discovering queries based on example tuples. In *Proceedings of the 2014 ACM SIGMOD International Conference on Management of Data*, SIGMOD '14, pages 493–504, New York, NY, USA, 2014. ACM.

[39] J. Shlens. A tutorial on principal component analysis. *arXiv preprint arXiv:1404.1100*, 2014.

[40] Sloan digital sky survey: Dr8 sample sql queries. `http://skyserver.sdss.org/dr8/en/help/docs/realquery.asp`.

[41] A. S. Szalay, P. Z. Kunszt, A. Thakar, J. Gray, D. R. Slutz, and R. J. Brunner. Designing and mining multi-terabyte astronomy archives: The sloan digital sky survey. In *SIGMOD Conference*, pages 451–462, 2000.

[42] B. Tang, K. Mouratidis, and M. L. Yiu. Determining the impact regions of competing options in preference space. In *Proceedings of the 2017 ACM International Conference on Management of Data*, SIGMOD '17, pages 805–820, New York, NY, USA, 2017. ACM.

[43] S. Tong and D. Koller. Support vector machine active learning with applications to text classification. *J. Mach. Learn. Res.*, 2:45–66, Mar. 2002.

[44] Q. T. Tran, C.-Y. Chan, and S. Parthasarathy. Query by output. In *Proceedings of the 2009 ACM SIGMOD International Conference on Management of Data*, SIGMOD '09, pages 535–548, New York, NY, USA, 2009. ACM.

[45] H. P. Vanchinathan, A. Marfurt, C. Robelin, D. Kossmann, and A. Krause. Discovering valuable items from massive data. In *Proceedings of the 21th ACM SIGKDD International Conference on Knowledge Discovery and Data Mining, Sydney, NSW, Australia, August 10-13, 2015*, pages 1195–1204, 2015.

[46] Z. Zhao, L. De Stefani, E. Zgraggen, C. Binnig, E. Upfal, and T. Kraska. Controlling false discoveries during interactive data exploration. In *Proceedings of the 2017 ACM International Conference on Management of Data*, SIGMOD '17, pages 527–540, New York, NY, USA, 2017. ACM.

APPENDIX

A. PROOFS OF FORMAL RESULTS

We show the proofs of propositions and theorems as follows.

Proof of Proposition 3.1:

PROOF. Since (1) $e_i^+ \in Q$ for $i = 1, \ldots, n^+$, (2) R^+ is the smallest convex set that contains L^+, and (3) Q is convex, we can derive that $R^+ \subseteq Q$, which means all points in R^+ are guaranteed to be positive. □

Proof of Proposition 3.2:

PROOF. Let us first prove that all points in each R_i^- are negative. Suppose that some point $\boldsymbol{x}_0 \in R_i^-$ is positive. According to the definition of R_i^-, $\overrightarrow{\boldsymbol{x}_0\boldsymbol{e}_i^-} \cap R^+ \neq \emptyset$, which means we can find a point $\boldsymbol{x}_1$ such that $\boldsymbol{x}_1 \in R^+$ and $\boldsymbol{x}_1 \in \overrightarrow{\boldsymbol{x}_0\boldsymbol{e}_i^-}$. Then $\boldsymbol{e}_i^-$ is on the line segment connecting two positive points $\boldsymbol{x}_0$ and $\boldsymbol{x}_1$. This contradicts the convex query assumption. Hence the supposition is false and all points in R_i^- are negative. Since R^- is just a union of all R_i^-'s, all points in R^- are negative as well. □

Proof of Theorem 3.1:

PROOF. At any iteration i, D_{eval} can be partitioned into D^+, D^- and D^u. Recall that D_{eval} is a projection of D_{test} without the labels. We know for certain that the labels for all points in D^+ (or D^-) are positive (or negative) in D_{test} according to Proposition 3.1, 3.2 and the definition of D^+ and D^- in Definition 3.4; only the labels for points in D^u are uncertain.

Let us assume that $p\%$ points in D^u are predicted as positive by the classifier trained at Line 14 of Algorithm 1. Denote the set of points as D^{u+}. Then $|D^{u+}| = p\% \cdot |D^u|$ and we can write the precision and recall of our DSM model as

$$\begin{aligned} precision &= \frac{|D^+| + |D^{u+} \cap Q|}{|D^+| + |D^{u+}|} = \frac{|D^+| + |D^{u+} \cap Q|}{|D^+| + p\% \cdot |D^u|} \\ &\geq \frac{|D^+|}{|D^+| + |D^u|} \\ recall &= \frac{|D^+| + |D^{u+} \cap Q|}{|D^+| + |D^u \cap Q|} \geq \frac{|D^+|}{|D^+| + |D^u|} \end{aligned}$$

F1-score is the harmonic mean of precision and recall. So F1-score is lower-bounded by $|D^+|/(|D^+| + |D^u|)$. □

Proof of Theorem 3.2:

PROOF. Since $(n\hat{p}, n\hat{q})^T$ follows Multinomial$(n, p, q, 1-p-q)$, the vector converges to the bivariate Normal distribution when n increases according to the Central Limit Theorem. Specifically,

$$\sqrt{n}\left(\begin{pmatrix}\hat{p}\\ \hat{q}\end{pmatrix} - \begin{pmatrix}p\\ q\end{pmatrix}\right) \xrightarrow{D} N\left(\begin{pmatrix}0\\ 0\end{pmatrix}, \Sigma\right)$$

where $\Sigma = \begin{pmatrix} p & -pq \\ -pq & q \end{pmatrix}$.

Define $v = (p, q)^T$, $\hat{v} = (\hat{p}, \hat{q})^T$, and $g(v) = \dfrac{p}{1-q}$. Then $b = g(v)$ and $X = g(\hat{v})$. According to the Delta method [8]

$$sup_\epsilon \|\Pr(\sqrt{n}|X_n - b| < \epsilon) - \int_{-\epsilon}^{\epsilon} \phi_{\sigma^2}(t)\mathrm{d}t\| = O(1/\sqrt{n})$$

where ϕ is the density function of the Normal distribution with mean zero and variance $\sigma^2 = (\partial g(v)/\partial v)^T \Sigma (\partial g(v)/\partial v) = p(1-p-q)/(1-q)^2$. Therefore, the theorem is proved. □

Proof of Proposition 3.3:

PROOF. Let X be the distance to B of a randomly chosen point from $\mathrm{D}_{unlabeled}$ and x_p be the distance such that $p = P(X > x_p)$. Let $X_1, \cdots, X_{m-k}$ be the distances to B of the instances in $\mathcal{U}$ at iteration k where k instances have been labeled. X_i's are a random sample of X, that is, a point in $\mathcal{U}$ is equally likely to be any one of the instances in $\mathrm{D}_{unlabeled}$.

Let Y_i be the distances to B of the ith instance in the sample of size l drawn from $\mathcal{U}$, $i = 1, \cdots, L$. Then

$$P(A|\mathcal{U}) = P(A|X_1, \cdots, X_{m-k}) = 1 - (1-\hat{p})^l$$

where $\hat{p} = P(Y_i > x_p|X_1, \cdots, X_{m-k}) = \frac{1}{m-k}\sum_{i=1}^{m-k} I\{X_i > x_p\}$. Note $E\hat{p} = EI\{X_i > x_p\} = P(X_i > x_p) = p$. Assume the entire database is large and ignore the correlation among the X_i's due to sampling without replacement. According to the Law of Large Numbers, $\hat{p}$ converges in probability to p and therefore

$$P(A|X_1 \cdots, X_{m-k}) = 1 - (1-\hat{p})^l \xrightarrow{p} 1 - (1-p)^l = 1 - \eta.$$

Further, According to the Central Limit Theorem, $\sqrt{m-k}(\hat{p} - p)$ converges in distribution to $N(0, p(1-p))$. In addition, with the Delta method,

$$\sqrt{m-k}(P(A|X_1 \cdots, X_{m-k}) - (1-\eta)) \xrightarrow{d} N(0, l^2 p(1-p)^{2l-1}).$$

k/m converges to zero as m goes to infinity. □

Proof of Proposition 4.1 and Proposition 4.2:

PROOF. If $R_f^+ \neq \emptyset$, for each point $\boldsymbol{x} = (\boldsymbol{x}_1, \cdots, \boldsymbol{x}_m) \in R_f^+$ where $\boldsymbol{x}_I$ denotes the values of $\boldsymbol{x}$ on attributes $\boldsymbol{A}_I$, we have $\boldsymbol{x}_I \in R_I^+$, $\forall I \in \mathbb{Z} \cap [1, m]$. According to proposition 3.1, all points in R_I^+ are positive for Q_I. Therefore, $\boldsymbol{x}$ is positive for $Q = Q_1 \wedge \cdots \wedge Q_m$. We prove that all points in the positive region R_f^+ are positive.

If $R_f^- \neq \emptyset$ and given a point $\boldsymbol{x} = (\boldsymbol{x}_1, \cdots, \boldsymbol{x}_m) \in R_f^-$, then there exists some subspace spanned by attributes $\boldsymbol{A}_I$ such that $\boldsymbol{x}_I \in R_I^-$. Since all points in R_I^- are negative for Q_I based on proposition 3.2, and the target query Q is in a conjunctive form, $\boldsymbol{x}$ is negative for Q. Therefore, we conclude that all points in the negative region R_f^- are negative.

To prove $R^+ \subseteq R_f^+$ and $R^- \subseteq R_f^-$, we consider the following three cases:

1. If $Q \in \mathbf{Q}_c^+$, then Q's positive region's projection onto each subspace is convex and we can build a convex polytope for the projection of the positive region in each subspace. We see that the Cartesian product of convex sets is convex, so R_f^+ is convex by definition. At each iteration, given a finite set of positive points $\{\boldsymbol{x}\}$, R^+ and R_f^+ are constructed on $\{\boldsymbol{x}\}$. Since R^+ as a convex polytope is the smallest convex set that contains $\{\boldsymbol{x}\}$, we conclude $R^+ \subseteq R_f^+$.

   To prove $R^- \subseteq R_f^-$, it is sufficient to prove that every arbitrary convex cone that R^- is built upon, is contained by R_f^-. Let $\boldsymbol{e}^-$ be the apex of a convex cone $R_{\boldsymbol{e}^-}^-$ in Definition 3.2. Since $\boldsymbol{e}^-$ is negative for Q, there exists I such that its factorization vector $\boldsymbol{e}_I^-$ is negative for Q_I. Let $\pi_I(R_{\boldsymbol{e}^-}^-)$ be the projection of the cone $R_{\boldsymbol{e}^-}^-$ onto the subspace spanned by $\boldsymbol{A}_I$. Then for a point $\boldsymbol{x} \in R_{\boldsymbol{e}^-}^-$, $\boldsymbol{x}_I \in \pi_I(R_{\boldsymbol{e}^-}^-)$.

   Now define the convex cone construction in the subspace spanned by $\boldsymbol{A}_I$ with $\boldsymbol{e}_I^-$ as apex as

   $$R_{\boldsymbol{e}_I^-}^- = \{\boldsymbol{x}_I \in \mathbb{R}^{d_I} | \overline{\boldsymbol{x}_I \boldsymbol{e}_I^-} \cap R_I^+ = \emptyset \wedge \overrightarrow{\boldsymbol{x}_I \boldsymbol{e}_I^-} \cap R_I^+ \neq \emptyset\}.$$

   We will now show that $\pi_I(R_{\boldsymbol{e}^-}^-) \subseteq R_{\boldsymbol{e}_I^-}^-$. We have $\pi_I(R_{\boldsymbol{e}^-}^-) = \{\boldsymbol{x}_I \in \mathbb{R}^{d_I} | \overline{\boldsymbol{x}_I \boldsymbol{e}_I^-} \cap \pi_I(R^+) = \emptyset \wedge \overrightarrow{\boldsymbol{x}_I \boldsymbol{e}_I^-} \cap \pi_I(R^+) \neq \emptyset\}$. Since $\boldsymbol{x}_I \in \pi_I(R_{\boldsymbol{e}^-}^-)$ and $\pi_I(R_{\boldsymbol{e}^-}^-)$ is a negative convex cone, $\overline{\boldsymbol{x}_I \boldsymbol{e}_I^-} \cap R_I^+ = \emptyset$ is true. On the other hand, since $\pi_I(R^+) \subseteq R_I^+$, $\overrightarrow{\boldsymbol{x}_I \boldsymbol{e}_I^-} \cap \pi_I(R^+) \neq \emptyset$ implies $\overrightarrow{\boldsymbol{x}_I \boldsymbol{e}_I^-} \cap R_I^+ \neq \emptyset$. This shows $\pi_I(R_{\boldsymbol{e}^-}^-) \subseteq R_{\boldsymbol{e}_I^-}^-$.

   Therefore $\boldsymbol{x}_I \in \pi_I(R_{\boldsymbol{e}^-}^-) \subseteq R_{\boldsymbol{e}_I^-}^- \subseteq R_I^-$, and $\boldsymbol{x} \in R_f^-$. Finally, $R_{\boldsymbol{e}^-}^- \subseteq R_f^-$ for any e^-, and hence $R^- \subseteq R_f^-$.

2. If $Q \in \mathbf{Q}_c^-$, the propositions can be proved by constructing DSM and DSM$_F$ in a reverse way such that we build a convex polytope for the negative region, and a union of convex cones for the positive region, one for each positive example.

3. If $Q \notin \mathbf{Q}_c$, then without factorization, DSM doesn't work and has $R^+ = \emptyset$, $R^- = \emptyset$. We therefore conclude $R^+ \subseteq R_f^+$ and $R^- \subseteq R_f^-$. In particular, for DSC queries, R_f^+ and R_f^- are nonempty regions. For p-DSC queries, although DSM can be built in each subspace, due to the conjunctive form of Q, $R_f^+ = \emptyset$ always holds true, but $R_f^- \neq \emptyset$ as long as there exists at least one subspace where $R_I^- \neq \emptyset$.

□

Proof of Proposition 4.3:

PROOF. Three-set metric is defined to be $\frac{|D^+|}{|D^+|+|D^u|} = \frac{|D^+|}{|D|-|D^-|}$. According to Proposition 4.1 and Proposition 4.2, both positive region and negative regions are enlarged by the factorized DSM, which speeds up the convergence of three-set metric. □

B. ALGORITHMS AND OPTIMIZATIONS

B.1 Extension of DSM

Categorical attributes. Inspired by the partitioning function that splits the data space into positive, negative, and unknown regions, our DSM extension for a categorical attribute partitions the domain (all possible constraints) of this attribute into the positive set (the constants that have been seen in positive examples), the negative set (the constants seen in negative examples), and the unknown set. For prediction over a new example, we check whether the attribute value in this example belongs to the positive (negative) set, and if so, give a prediction of Yes or No. If the attribute value belongs to the unknown set, we pass the example to the classifier for final prediction. In case of noisy labeling, we also maintain a counter of the conflicting examples seen thus far regarding the positive and negative sets of constants stored. For instance, if the color 'red' of a vehicle is in the positive set, but later we see the color 'red' added to the negative set, we count it as a conflicting example. When the counter exceeds the threshold T, we use the classifier as a fallback to handle this categorical attribute.

B.2 Dimensionality Reduction Methods

In our work, we examine a range of popular feature selection techniques in our active learning framework for data exploration. These techniques are provided by the scikit-learn library[6]:

Principled Component Analysis (PCA) defines a set of orthogonal directions that capture the maximum variance of a dataset, with an implicit hope that the variance along a small number of

[6] http://scikit-learn.org/stable/

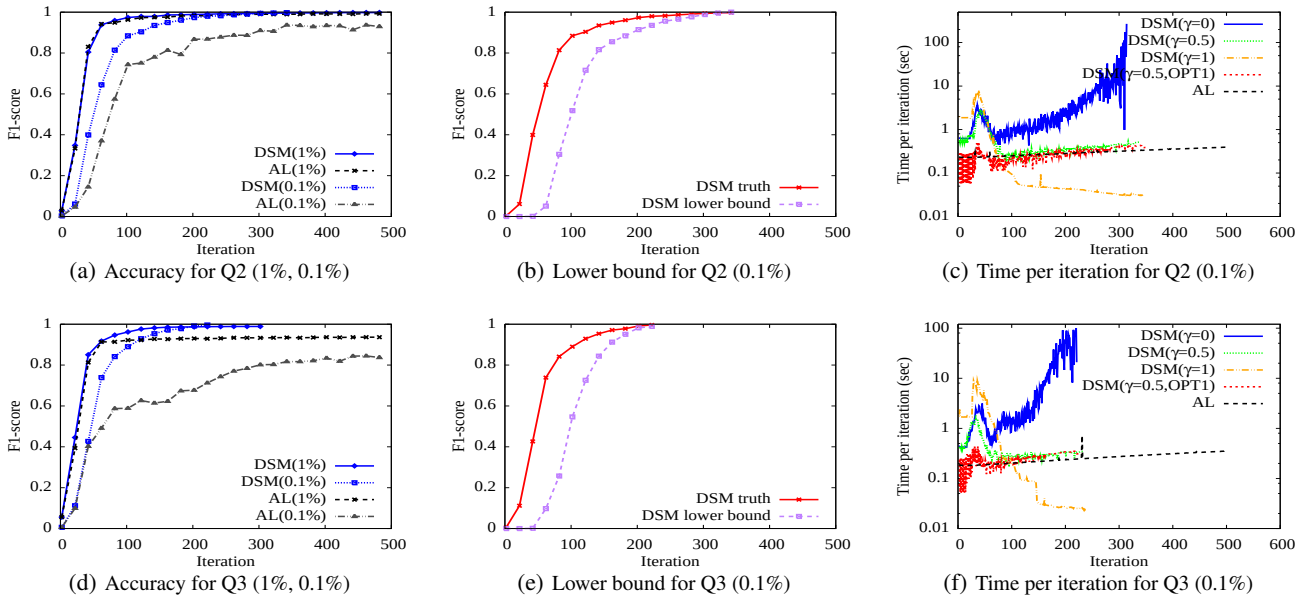

(a) Accuracy for Q2 (1%, 0.1%) (b) Lower bound for Q2 (0.1%) (c) Time per iteration for Q2 (0.1%)

(d) Accuracy for Q3 (1%, 0.1%) (e) Lower bound for Q3 (0.1%) (f) Time per iteration for Q3 (0.1%)

Figure 7: Additional results of DSM for 2D user interest queries.

principal components provides a reasonable characterization of the entire dataset [39]. In our work, PCA is used as a query-agnostic dimensionality reduction technique. That is, we use it to compress a database table $D(A_1, \ldots, A_d)$ into a new table $D'(B_1, \ldots, B_k)$ with fewer columns, $k < d$. Each database object has two presentations using $(A_1, \ldots, A_d)$ and $(B_1, \ldots, B_k)$, respectively. In each iteration of data exploration, we display a new sample to the user using the $D(A_1, \ldots, A_d)$ representation, but train an SVM with all existing labeled samples on $D'(B_1, \ldots, B_k)$.

Random forests (RF) are an ensemble learning method that operates by constructing a multitude of decision trees at training time and outputting the mean prediction of the individual trees.

Gradient boosting regression trees (GBRT) are a gradient boosting machine with decision trees as base-learners. The basic idea is to construct a series of decision trees in a forward stagewise manner, where each new decision tree is constructed to be maximally correlated with the negative gradient of the loss function – the error of the whole ensemble learnt so far. The additive model of GBRT is a linear combination of the base learners.

Our work uses RF and GBRT for online feature selection. The evaluation results of these methods are shown in Appendix C.

B.3 Final Result Retrieval

Once the exploration terminates, we obtain a DSM model represented by its decision boundary H.

Our goal is to find all tuples in the database D with positive predictions by this model, i.e., $\boldsymbol{x}$ such that $\boldsymbol{x} \in D$ and $H(\boldsymbol{x}) > 0$. To expedite the retrieval, we propose to build R-tree as the index on the database, and perform depth-first search from the root.

Branch and Bound. The unique aspect of the R-tree search is a solver-based branch and bound approach. Each R-tree node offers a hyper-rectangle as a minimum bounding box of all the data points reachable from this node. With the decision function $H(\boldsymbol{x})$ as defined in Section 4, we can compute an upper bound of $H(\boldsymbol{x})$ without visiting the descendant nodes. Instead, we can obtain it by solving the following constraint optimization problem.

$$\begin{aligned} \max_{\boldsymbol{x}} \quad & H(\boldsymbol{x}) \\ \text{s.t.} \quad & a_j \le \boldsymbol{x}^{(j)} \le b_j,\ j = 1, \ldots, d. \end{aligned} \tag{6}$$

where $[a_j, b_j]$ is the range of the tree node on the j-th dimension and $\boldsymbol{x}^{(j)}$ is the value of $\boldsymbol{x}$ on the j-th dimension. If the upper bound is less than 0, we can prune the entire subtree rooted at this node. Since the positive results tend to be clustered and cover a small portion of the database, with such an index we may save cost than scanning the entire database and running the model on each tuple.

C. ADDITIONAL EVALUATION RESULTS

Servers: Our experiments were run on five identical servers, each with 12-cores, Intel(R) Xeon(R) CPU E5-2400 0 @2.4GHz, 64GB memory, JVM 1.7.0 on CentOS 6.6.

C.1 More Results on Dual-Space Algorithm

Active Search. We first provide more details on the Active Search (AS) algorithm that we compare DSM to.

Algorithm. Active search aims to maximize the number of positive examples discovered, called the *target set accuracy*, within a limited budget of user labeling effort. In contrast, active learning aims to maximize the *classification accuracy*, and specifically, our active learning based approach maximizes the *F1-score* of the model $H(x)$ learned to approximate the true user interest $Q(x)$: $\{x\} \rightarrow \{-1, 1\}$, which assigns a positive or negative label to each database example. Given the difference in optimization objective, it is not surprising to see that active search algorithms tend to find new examples that are "similar" or "close" to existing positive examples, while attempting to strike a balance between exploiting the most probable region of positive examples and exploring broadly to discover new regions of positive examples (exploitation versus exploration). In contrast, active learning based algorithms like ours tend to discover and refine the decision boundary between the positive class and negative class of examples, and hence sample often around the current decision boundary and from **both** classes.

The Active Search (AS) algorithm in [17] assumes that it is already given a classification model $\mathbb{P}(y = 1|x, D_{labeled})$, which returns the probability of an unlabeled example x taking the label $y = 1$ based on the current labeled set $D_{labeled}$. At any given iteration, to propose a new example for labeling from the unlabeled

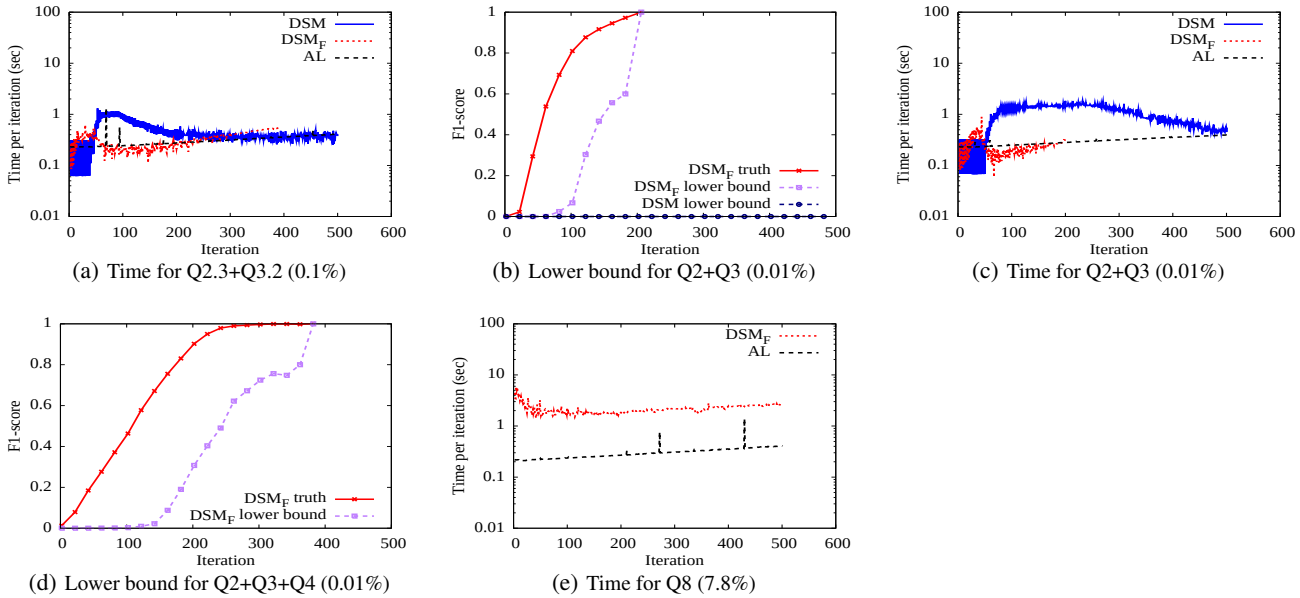

(a) Time for Q2.3+Q3.2 (0.1%) (b) Lower bound for Q2+Q3 (0.01%) (c) Time for Q2+Q3 (0.01%)

(d) Lower bound for Q2+Q3+Q4 (0.01%) (e) Time for Q8 (7.8%)

Figure 8: Additional results of DSM with factorization for 4D and 6D user interest queries.

set, the AS algorithm chooses the example that maximizes the expected utility (i.e. the number of positive points retrieved) in the next t steps:

$$\arg\max_{x \in D_{unlabeled}} \mathbb{E}[y_1 + \ldots + y_t | x, D_{labeled}]$$

There are two specific cases to consider: (1) By choosing $t = 1$, the algorithm becomes a greedy one, i.e., retrieving the example with the highest probability of being positive. (2) As we increase the lookahead parameter t, the algorithm starts to gain the ability to explore a region where the immediate reward is lower but there is a chance of discovering more targets overall in the next t steps. While a dynamic programming procedure can be employed, the t-step lookahead algorithm is still computationally expensive, with an exponential cost in the unlabeled set size per iteration.

In order to reduce the runtime complexity, a branch-and-bound optimization was introduced in [17], which works for a specific kNN classifier, referred to as a *static* kNN classifier:

$$P(y = 1 | x, D_{labeled}) = \frac{\gamma + \sum_{i \in \text{L-kNN}(x)} y_i}{1 + \sum_{i \in \text{L-kNN}(x)} 1}$$

where L-kNN(x) is the intersection between of the k-nearest neighbors of x in the entire dataset and the examples in $D_{labeled}$, and γ is a smoothing constant. Under this model, an optimization procedure can be used to restrict the search of the optimal example for labeling to a small subset of them, speeding up the computation and allowing to use a higher value of t in practice.

We implemented both the greedy algorithm and the t-step lookahead algorithm with the branch-and-bound optimization based on a static kNN classifier.

Hyper-parameter tuning. The active search algorithm involves several parameters. First, the static-kNN classifier includes two hyper-parameters: the number of neighbors k and the smoothing parameter γ. For γ, we used $\gamma = 0.1$, the same value as suggested in the original paper [17]. As for k, we performed parameter tuning by varying $k = 50$ (default in [17]), 100, 500, 1000. We observed that higher values of k return better F-score, but also increase memory consumption quickly because the space complexity for storing the k-nearest neighbors is of $O(kN)$, where N is the number of points in the dataset. In our case, where N = 1.9 million and k = 500, it can easily consume dozens of GB of memory, while k = 1000 would cause an out-of-memory error. Therefore we used $k = 500$ in our experiments.

The algorithm in [17] also has the lookahead parameter t as described above. The original paper reported little difference in accuracy between t=1, 2, and 3 before 200 labeled examples, which was confirmed in our experiments as well. However, increasing t would increase the per-iteration time cost quickly. We could barely achieve interactive performance for t=2 over the SDSS dataset. Due to the performance reason we did not go beyond 2-step lookahead in our experiments.

Analysis of Performance. The performance of active search is shown in Figure 5 and Figure 6(a) for 2D, 4D, and 6D queries. We provide additional analysis below.

(1) Why Active Search is worse than Active Learning: AS performs much worse than AL-KNN$^+$ while both use the kNN classifier. The main reason is that AS uses a strategy to maximize the positive examples in the selected examples, but not the classification accuracy. So it tends to sample new examples close to existing positive ones, as stated earlier. In comparison, AL aims to maximize classification accuracy by sampling the most uncertain region of the model, which provides better F1-score. In addition, AS uses a static kNN classifier, denoted as KNN$^-$, which builds a fixed kNN structure over the database in advance. Then during data exploration, in each iteration it computes the intersection of the fixed kNN structure of a point x with the labeled examples and does majority voting from the labeled neighborhood of x to predict its label. Before the user has labeled enough examples, the labeled neighborhood of x is quite sparse and hence not as accurate for prediction. In contrast, AL-KNN$^+$ builds the labeled neighborhood of any x dynamically by finding the k closest points from the current labeled examples, hence offering better performance of the classifier.

(2) Target set accuracy observations: As Figure 9 shows, Active Search is more efficient at retrieving positive points from the dataset than Active Learning and DSM for the 2D queries. However, as the dimensionality grows, we observe the reverse: DSM and Active Learning outperform Active Search in retrieving posi-

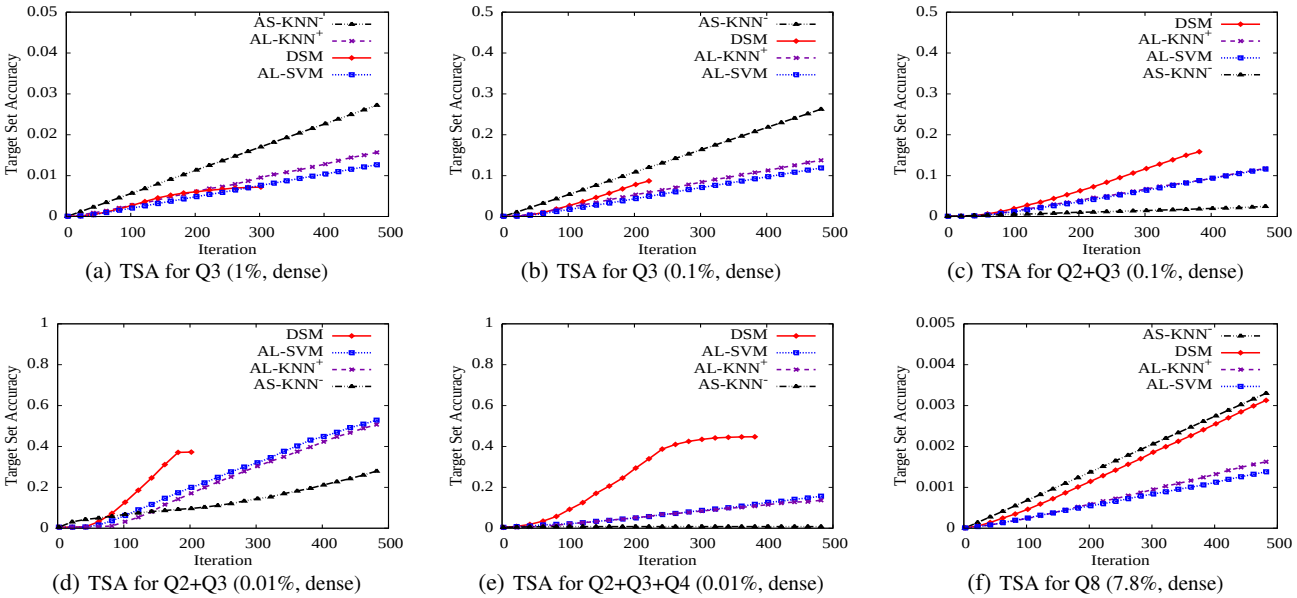

(a) TSA for Q3 (1%, dense) (b) TSA for Q3 (0.1%, dense) (c) TSA for Q2+Q3 (0.1%, dense)

(d) TSA for Q2+Q3 (0.01%, dense) (e) TSA for Q2+Q3+Q4 (0.01%, dense) (f) TSA for Q8 (7.8%, dense)

Figure 9: Target Set Accuracy(TSA) for SDSS queries.

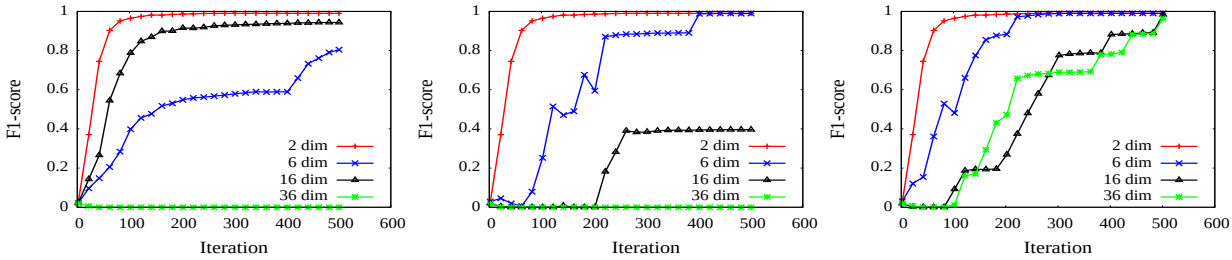

(a) Principled Component Analysis (PCA) (b) Random Forests (c) Gradient Boosting Regression Trees

Figure 10: Compare Dimensionality Reduction and Feature Selection techniques for learning Query 2.2 using a SDSS 66k dataset.

tive points as the iterations progress. This could be explained by two factors. First, these methods are based on different classifiers: SVM is least sensitive to dimensionality while kNN is more so due to the degradation of the distance function in high-dimensional space. Further, the dynamic kNN tends to give better accuracy than the static kNN. Secondly, DSM can determine whether a point is positive or negative without asking the user to label, possibly obtaining "more than one positive point" per iteration.

C.2 More Results on Feature Selection

In this section, we present additional results on feature selection when the data exploration starts with irrelevant attributes.

We consider three dimensionality reduction methods: PCA as a database compression method, and Random Forests (RF) and Gradient Boosting Regression Trees (GBRT) for online feature selection. They were described in detail in Appendix B.2. To understand the best achievable performance, we fed the true number of relevant attributes to the online feature selection algorithms, and used a full scan of the dataset to find the point closest to the decision boundary in each iteration. Given the slow performance of some algorithms, we used a smaller 66k-tuple dataset. As Figure 10 shows, our results shown that F-scores of PCA and RF for 36-dimensions stay close to 0, while GBRT can achieve over 95% with 500 examples (if the number of relevant attributes is fed to it).

C.3 More Results on System Comparison

We compare our system to two state-of-the-art systems on explore-by-example: (1) **Aide** [13, 14] uses decision trees as the classification model. If a query pattern is non-linear, it uses a collection of hyper-rectangles in the data space to approximate the pattern. We obtained the source code from the authors. (2) **LifeJoin** [10] reports a method, named "hybrid", as its best performing method. At each iteration, it uses all the labeled examples to train a collection of weak-learners (error-free regarding the training data), extracts basic predicates from these learners, and trains a **linear** SVM over these predicates. Then the SVM is used to seek the next example for labeling, which is the one closest to the SVM boundary. The final retrieval method collects the support vectors of the final SVM, uses it as a training set to build a decision tree, and converts the positive class of the decision tree to a query to retrieve all the objects. We reimplemented the LifeJoin with two modifications: we used Random Forest (RF) with overfitted decision trees to build the weak learns as RF is a better known approach than a program synthesizer for this purpose, and we used our sample retrieval method to find the one closest to the SVM boundary, avoiding scanning the entire dataset. We made parameters consistent with those recommended in the paper, including the number of weak learners used (10) and the number of basic features (on the order of hundreds).

In our experiments, LifeJoin and DSM use the same seeds as they are implemented in the same framework. AIDE has a standalone codebase. It uses a k-means based exploration method for skewed data. Hence, it uses its own seeds to discover cluster centroids and

Table 3: Final retrieval in our system, Aide and LifeJoin.

Query	Metrics	LifeJoin	AIDE	B&B	Scan
Q1 (0.1%)	F-score (%)	7.13 (45.12)	95.8	88.0	88.0
	Time (s)	0.683	0.013	79.7	1009.2
Q2 (0.1%)	F-score (%)	48.81 (58.76)	86.5	93.9	92.3
	Time (s)	0.338	0.018	104.3	1023.8
Q5 (0.01%)	F-score (%)	0.02 (0.0)	4.6	84.9	84.6
	Time (s)	2.575	0.088	207.2	1039.7

samples around the centroids. When comparing these systems, we exclude the overhead to find the first initial example as these systems use different methods/assumptions to find this initial example.

Finally, Table 3 shows the final result retrieval after 500 iterations and compares the three systems in both accuracy and running time. Again, LifeJoin suffers from low accuracy, using either its decision-tree based final retrieval method or running the SVM model over the database (in parentheses). Aide loses accuracy for workloads beyond 2D. Finally, our system uses the Branch-and-Bound ("B&B") optimization described in Appendix B.3. It is shown to significantly reduce the retrieval time compared a full scan ("Scan") Our system maintains high accuracy by maintaining a more complex model, while having a modest final retrieval time of a few minutes.

C.4 More on the User Study

We downloaded a dataset of cars from http://www.teoalida.com/. It contains 5622 vehicles from 407 models of 43 different makes between 2016 and 2018. Each vehicle is described by a unique identifier and attributes about the engine, the transmission, the warranty, etc. There were a lot of missing values. We manually checked authoritative websites such as Edmunds to fill in missing values. Moreover, we downloaded retail prices through the Edmunds API. After data cleaning, we had 27 attributes with sufficient data for data exploration. Among these attributes, 15 of them are numerical attributes and 12 are categorical attributes.

Note that in the study, we asked the user to manually try different SQL queries, for which we used the original 27 attributes. When we ran the simulation using our active learning system, we used the transformed dataset with *one-hot encoding* because most classifiers require the categorial attributes to be transformed using one-hot encoding. In such transformation a categorical attribute with k values is transformed to k features, with one feature per distinct value. This can increase 27 attributes in our dataset to 547 features in total. We perform above transformation on demand when the user chooses the attributes for exploration and the database sample is loaded into memory.

Below, Table 4 records the detailed queries from the user study, and Figure 11 shows the performance of traditional SVM-based active learning and DSM for these queries.

Comparison to Active Learning. As can be seen, our DSM algorithm outperforms active learning for all the queries, with drastic performance gains for Q2, Q4, Q5, Q7, Q10, Q11, Q13, Q14, Q15, Q17. AL cannot reach 99% accuracy for most queries within 100 iterations, and it cannot reach 95% accuracy for half of the queries, while DSM reaches 99% with 10 labeled examples. Detailed profiling results reveal the following reasons: 1) *Class imbalance*: All queries have selectivity 0.9% or less. The classifier tends to ignore the minority class despite parameter tuning. A few misclassifications lead to high loss in F1-score. 2) *Uncertainty sampling* tends to select training examples close to the decision boundary. Sometimes, the distance between positive examples can be larger than the distance between positive and negative examples, which confuses a large-margin classifier. 3) *Data distribution* can be so sparse that the positive examples for a convex query appear to be several disjoint regions, which confuses the classifier, and uncertainty sampling cannot fix the issue. In contrast, DSM samples from the dual-space model, not just the boundary of the classifier.

Noisy labels. We furhter consider noisy labels to test the robustness of DSM, whose implementation is described in §4. Any polytope model that has exceeded T=2 conflicting examples will be turned off and fall back to the classifier. To inject noisy labels, our intuition is that they are more likely to occur close to the boundary of the true pattern. 1) *Noise model*: we use both a *random* noise model where p (=0.1 or 0.2) controls the probability of having a wrong label, and a *Gaussian* noise model where a new example gets a wrong label with a probability that depends on its distance to the true boundary, i.e., the probability that its distance to the boundary of a perfect SVM classifier (with the margin size δ) is less than a sample from a Gaussian function with u=0 and $\sigma = \delta/2$. 2) *Non-uniform user behaviors*: we assume the first s (=5 or 10) examples to be noise free because they are drawn from the broad data space, hence likely to be far from from the true boundary, and the user tends to be more patient at the beginning. The last 9 columns of Table 5 show DSM and AL under noisy labels. With a median of 11 labeled examples, DSM can reach 95% accuracy with 5 noise-free initial examples, and with a median of 10 labeled examples, it can reach 99% with 10 noise-free examples, while AL can at most achieve 80% with 36 labeled examples. DSM is more resistant to noisy labeling due to its fast convergence.

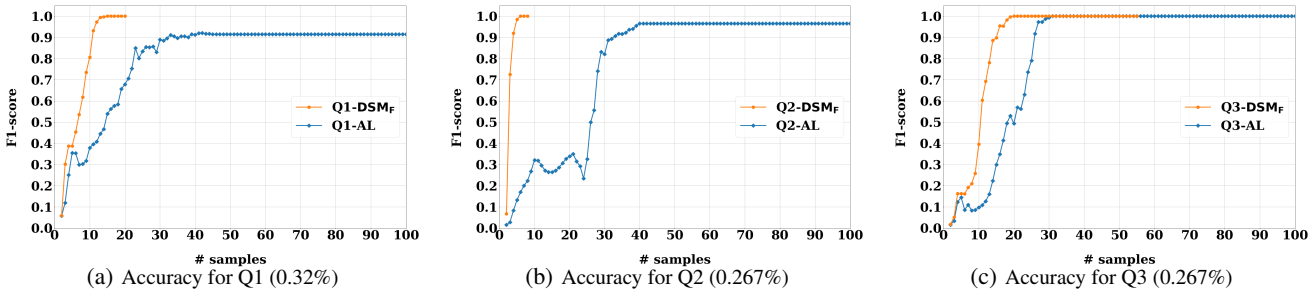

(a) Accuracy for Q1 (0.32%)

(b) Accuracy for Q2 (0.267%)

(c) Accuracy for Q3 (0.267%)

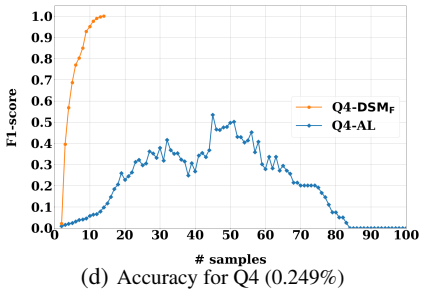

(d) Accuracy for Q4 (0.249%)

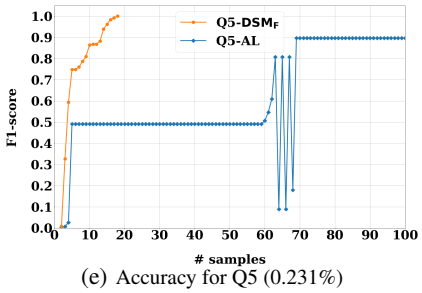

(e) Accuracy for Q5 (0.231%)

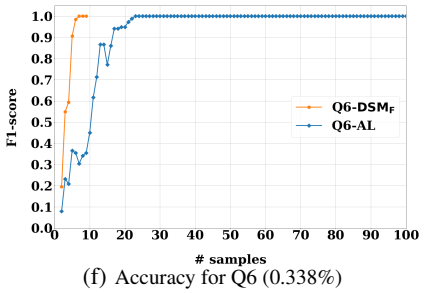

(f) Accuracy for Q6 (0.338%)

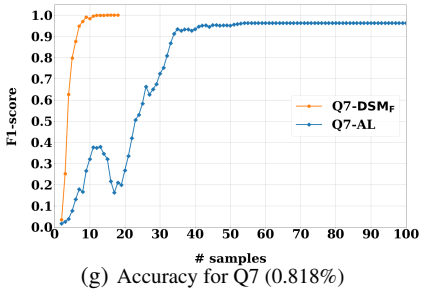

(g) Accuracy for Q7 (0.818%)

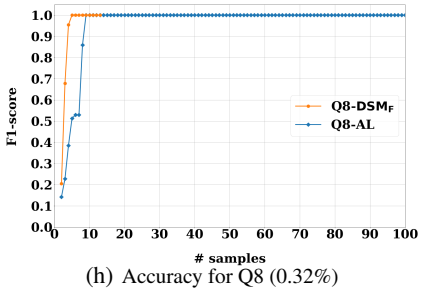

(h) Accuracy for Q8 (0.32%)

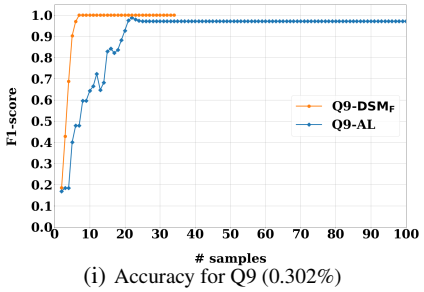

(i) Accuracy for Q9 (0.302%)

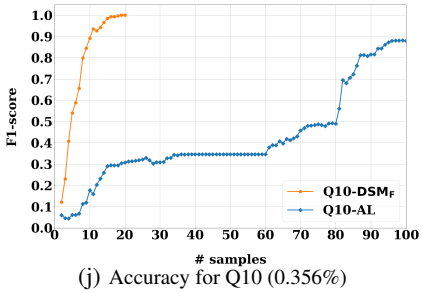

(j) Accuracy for Q10 (0.356%)

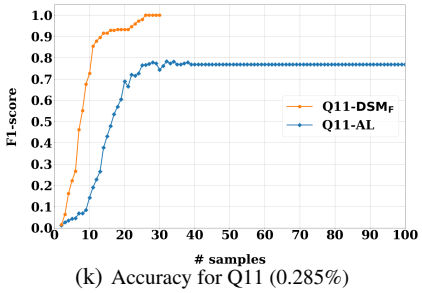

(k) Accuracy for Q11 (0.285%)

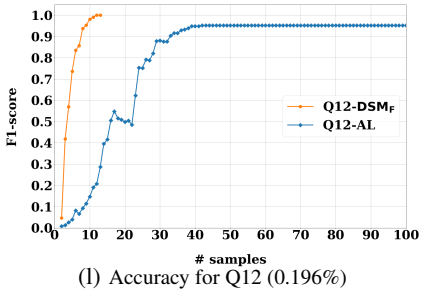

(l) Accuracy for Q12 (0.196%)

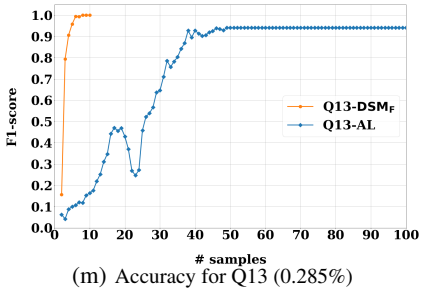

(m) Accuracy for Q13 (0.285%)

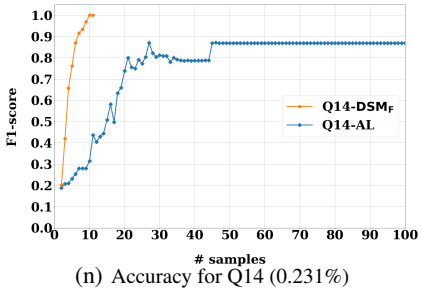

(n) Accuracy for Q14 (0.231%)

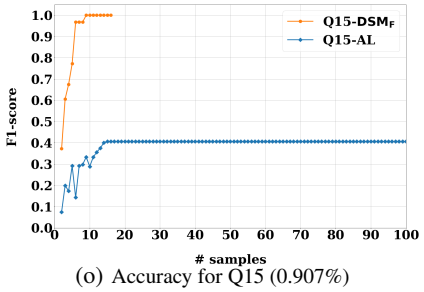

(o) Accuracy for Q15 (0.907%)

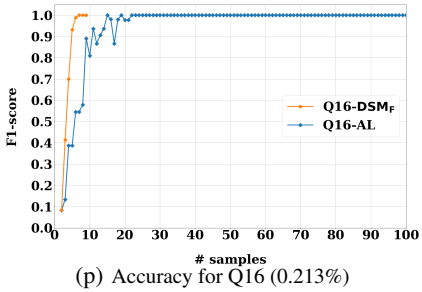

(p) Accuracy for Q16 (0.213%)

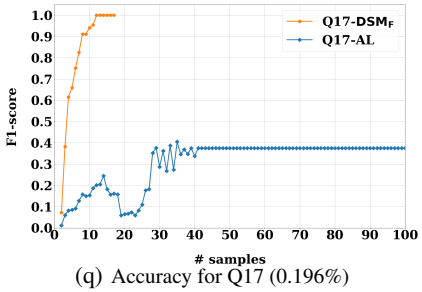

(q) Accuracy for Q17 (0.196%)

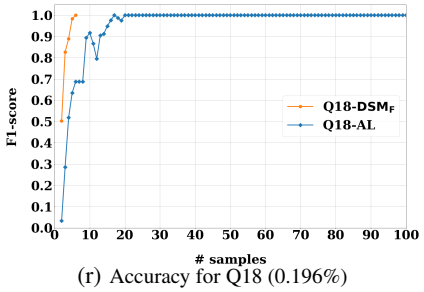

(r) Accuracy for Q18 (0.196%)

Figure 11: Accuracy for 18 queries in the Cars User Study(No noise).

Table 4: True Queries obtained from the Cars User Study

Query	Predicate
1	class = 'minivan' **AND** price_msrp $\leq$ 30000 **AND** length $>$ 5 **AND** length * width $>$ 10.1 **AND** fuel_type = 'regular unleaded' **AND** transmission ! $=$ '8-speed shiftable automatic' **AND** transmission ! $=$ '9-speed shiftable automatic'
2	price_msrp $\leq$ 22132 **AND** basic_year $\geq$ 5 **AND** drivetrain_year $\geq$ 10 **AND** horsepower $>$ 156 **AND** body_type != 'suv' **AND** transmission = '6-speed shiftable automatic' **AND** year $\geq$ 2016 **AND** fuel_tank_capacity $\geq$ 65
3	year $\geq$ 2016 **AND** length * height * width $\geq$ 15.0 **AND** basic_year $\geq$ 4 **AND** class = 'full-size car' **AND** price_msrp $<$ 100000 **AND** engine_type = 'gas'
4	body_type = 'truck' **AND** height $\geq$ 1.9 **AND** torque $\geq$ 3800 **AND** price_msrp $\leq$ 30000 **AND** year = 2017 **AND** base_engine_size $\geq$ 5
5	class = 'full-size van' **AND** body_type = 'van' **AND** engine_type = 'gas' **AND** model = 'nv cargo' **AND** price_msrp $<$ 27000 **AND** horsepower $<$ 300
6	height $<$ 1.51 **AND** drivetrain_year $\geq$ 10 **AND** transmission ! $=$ '6-speed manual' **AND** transmission ! $=$ '7-speed manual' **AND** class = 'subcompact car'
7	class = 'mid-size car' **AND** transmission = '6-speed shiftable automatic' **AND** drivetrain_year $>$ 5 **AND** price_msrp $<$ 29000 **AND** basic_km $\geq$ 80467 **AND** body_type != 'suv'
8	length $\geq$ 6 **AND** body_type != 'sedan' **AND** fuel_type != 'premium unleaded (recommended)' **AND** drive_type != 'front wheel drive' **AND** fuel_type != 'premium unleaded (required)' **AND** basic_year $\geq$ 4 **AND** drivetrain_year $\geq$ 5 **AND** price_msrp $<$ 32000 **AND** height $>$ 2.5
9	(body_type = 'truck' **OR** body_type = 'van') **AND** price_msrp $<$ 30000 **AND** height $\geq$ 2.5 **AND** length $>$ 6
10	body_type = 'truck' **AND** horsepower $>$ 350 **AND** drive_type = 'four wheel drive' **AND** engine_type != 'diesel' **AND** fuel_tank_capacity $>$ 100 **AND** year $\geq$ 2017 **AND** suspension != 'stabilizer bar stabilizer bar' **AND** price_msrp $<$ 35000
11	(body_type = 'suv' **OR** body_type = 'truck') **AND** (drive_type = 'all wheel drive' **OR** drive_type = 'four wheel drive') **AND** height $>$ 1.8 **AND** price_msrp $<$ 33000 **AND** length $>$ 5.9 **AND** suspension like '%independent%'
12	price_msrp $<$ 25000 **AND** horsepower $>$ 200 **AND** year = 2017 **AND** length $>$ 5.5
13	price_msrp $<$ 23000 **AND** basic_year $\geq$ 5 **AND** drivetrain_year $\geq$ 10 **AND** basic_km $\geq$ 80000 **AND** drivetrain_km $\geq$ 100000 **AND** engine_type **IN** ('gas', 'hybrid') **AND** body_type **IN** ('sedan', 'hatchback') **AND** drive_type = 'front wheel drive' **AND** fuel_tank_capacity $\geq$ 55 **AND** year $\geq$ 2017
14	price_msrp $<$ 13000 **AND** drive_type = 'front wheel drive' **AND** transmission **LIKE** '%manual%' **AND** length $<$ 4.5 **AND** horsepower $<$ 110
15	transmission **LIKE** '%automatic%' **AND** price_msrp $<$ 25000 **AND** class **NOT LIKE** '%pickup%' **AND** class **NOT LIKE** '%suv%' **AND** basic_year $\geq$ 4 **AND** year $\geq$ 2017 **AND** height $\leq$ 1.62
16	price_msrp $<$ 26000 **AND** body_type **IN** ('van', 'truck') **AND** height $<$ 2.5 **AND** height $>$ 2 **AND** basic_year $>$ 3
17	horsepower $>$ 150 **AND** year = 2017 **AND** make **IN** ('hyundai', 'honda') **AND** length $<$ 4.5 **AND** engine_type **IN** ('gas', 'diesel') **AND** price_msrp $<$ 20000
18	price_msrp $<$ 30000 **AND** body_type **IN** ('sedan', 'suv') **AND** engine_type = 'hybrid' **AND** year = 2017 **AND** basic_year $\geq$ 5 **AND** drivetrain_year $\geq$ 10

Table 5: Results of the car database using Manual Exploration, DSM, Active Learning (AL). # A shows the number of attributes used in the user interest and # F shows the number of features (with onehot encoding) after transforming all categorical attributes for use by the classifier. For manual exploration, T_2 shows the number of tuples reviewed in initial exploration (the 2nd phase) for the user to find the first positive example; and T_3 shows those reviewed in iterative exploration (3rd phase). For DSM and AL, the algorithm marked by '-' never reached the desired accuracy within 100 iterations.

Q	**# A**	**# F**	**Manual Exploration**			**AL**			**DSM**			**DSM: 5 noise free**			**DSM: 10 noise free**			**AL: 10 noise free**		
			T_2	T_3	#SQL	0.8	0.95	0.99	0.8	0.95	0.99	0.8	0.95	0.99	0.8	0.95	0.99	0.8	0.95	0.99
1	6	58	0	122	20	23	-	-	10	12	13	10	-	-	10	20	-	35	-	-
2	8	37	13	104	49	29	39	-	4	5	6	4	5	6	4	5	6	37	-	-
3	8	35	8	193	29	26	27	30	14	16	19	30	-	-	14	-	-	30	-	-
4	6	14	17	52	17	-	-	-	7	10	13	7	11	14	7	10	13	-	-	-
5	6	418	18	80	10	63	-	-	9	15	17	-	-	-	9	19	-	-	-	-
6	4	49	12	67	8	13	21	23	5	6	7	5	-	-	5	6	7	-	-	-
7	6	59	2	187	16	32	42	-	6	8	9	6	8	-	6	8	9	33	49	-
8	8	26	11	202	17	8	9	9	4	4	5	4	4	5	4	4	5	8	9	9
9	4	12	11	35	8	15	21	-	5	6	7	5	11	14	5	6	7	20	56	-
10	8	31	3	47	11	87	-	-	9	14	16	8	13	-	9	13	-	98	-	-
11	6	26	16	412	11	-	-	-	11	23	26	11	30	-	11	24	94	32	-	-
Min	4	12	0	35	8	8	9	9	4	4	5	4	4	5	4	4	5	8	9	9
Max	8	418	18	412	49	-	-	-	14	23	26	-	-	-	14	-	-	-	-	-
Mdn	6	35	11	104	16	29	42	-	7	10	13	7	13	-	7	10	13	35	-	-
12	4	4	24	75	15	28	42	-	6	9	11	6	-	-	6	9	11	31	-	-
13	10	24	4	158	13	35	-	-	4	5	6	4	5	6	4	5	6	91	-	-
14	5	29	1	50	4	26	-	-	6	9	10	6	10	12	6	9	10	48	-	-
15	6	51	1	91	10	-	-	-	6	6	9	6	6	-	6	6	9	-	-	-
16	4	12	7	260	12	9	15	15	5	6	7	5	6	-	5	6	7	9	16	-
17	6	49	12	108	7	-	-	-	7	11	12	-	-	-	7	11	12	-	-	-
18	6	17	4	81	6	9	16	17	3	5	6	3	5	6	3	5	6	9	-	-
Min	4	4	1	50	4	9	15	15	3	5	6	3	5	6	3	5	6	9	16	-
Max	10	51	24	260	15	-	-	-	7	11	12	-	-	-	7	11	12	-	-	-
Mdn	6	24	4	91	10	28	-	-	6	6	9	6	6	-	6	6	9	48	-	-
$\mathbf{Min_g}$	4	4	0	35	4	8	9	9	3	4	5	3	4	5	3	4	5	8	9	9
$\mathbf{Max_g}$	10	418	24	412	49	-	-	-	14	23	26	-	-	-	14	-	-	-	-	-
$\mathbf{Mdn_g}$	6	30	9.5	97.5	11.5	28.5	-	-	6	8.5	9.5	6	11	-	6	8.5	9.5	36	-	-